Waveguide Antenna Array for Automotive Radar

Master Thesis
submitted to the Faculty of the
Escola Tècnica d'Enginyeria de Telecomunicació de Barcelona
Universitat Politècnica de Catalunya
by

Roger Vela González

In partial fulfillment
of the requirements for the master in
MASTER'S DEGREE IN TELECOMMUNICATIONS **ENGINEERING**

Contents

List of Figures

List of Tables

Revision history and approval record

Revision	Date	Purpose
0	15/09/2022	Document creation
1	17/01/2023	Document revision
2	20/01/2023	Document revision

DOCUMENT DISTRIBUTION LIST

Name	e-mail
Roger Vela González	
doc. Ing. Juan-Manuel Rius Casals, Ph.D.	
doc. Ing. Pavel Hazdra, Ph.D.	
Ing. Jan Kraček, Ph.D.	

Written by:		Reviewed and approved by:	
Date	15/09/2022	Date	17/01/2023
Name	Roger Vela González	Name	Juan-Manuel Rius Casals
Position	Project Author	Position	Project Supervisor

Abstract

Automotive radars can use the wide band at extremely high frequencies (EHF) between 30 GHz and 300 GHz, which has a higher amount of free frequency bands than the lower part of the electromagnetic spectrum. The focus of this thesis is to develop a horn antenna to work in this band with the central frequency of 77 GHz, a Field of View (FOV) of 20º on Elevation and 130º on Azimuth and a reflection coefficient (S11) below -15 dB. It was possible to accomplish the requirements set by the company with a single horn antenna, which is a less complex and more compact solution. This thesis presents the results with a brief review of a two-element antenna array for possible future works.

1 Introduction

1.1 Project Description

This thesis aims to design a low sidelobe level waveguide antenna array for automotive radar working at the frequency of 77 gigahertz (GHz). This work is based on the requirements given by the Valeo company.

1.2 Statement of purpose

The objectives defined at the beginning of the project are the following:

1. Become familiar with professional software used to design antennas.

2. Identification and exploration of the critical requirements and parameters related to the performance of a waveguide antenna array for automotive radar working at the frequency of 77 GHz.

3. Design of a waveguide antenna array for automotive radar working at the frequency of 77 GHz.

1.3 Requirements and specifications

The requirements for the antenna design agreed upon with the company at the beginning of the project were:

1. Operating frequency between 76 GHz and 80 GHz.

2. Central frequency at 77 GHz.

3. Elevation beamwidth from -10$^{\text{o}}$ to 10$^{\text{o}}$.

4. Azimuth beamwidth from 25$^{\text{o}}$ to 155$^{\text{o}}$.

5. S11 < -15 dB

6. Sidelobes > 15 dB apart

7. -30 dB cross polarization in the main direction

8. Lobe variations $\pm$2 dB in the main lobe

1.4 Methods and procedures

This project was started by the need of a company to create an antenna system working at 77 GHz with the requirements stated in the previous section. It is based on the literature review of the bibliography indicated in the bibliography section, with the main one being "Electromagnetic Waves and Antennas" by Sophocles J. Orfanidis from the Rutgers University. Besides, the project is accomplished by using software Antenna Magus and CST Studio Suite, both by Dassault Systemes.

1.5   Gantt Diagram
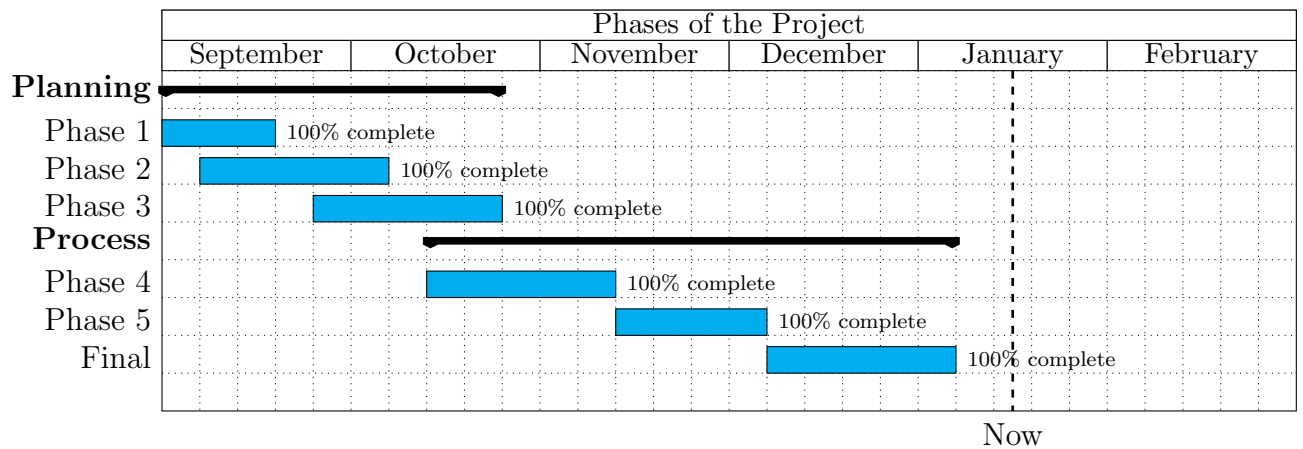
Figure 1: Gantt diagram of the project

The different Phases of the Gantt diagram refer to the following:

- Phase 1: Project definition

- Phase 2: Literature review

- Phase 3: Software familiarization

- Phase 4: Design of prototypes with a focus on the field of view.

- Phase 5: Design of prototypes with a focus on Adaptation.

- Final: Design of final prototype.

1.6   Deviations from initial plan

As the project description and objectives state, the initial plan for this project was that the antenna created would be an array of two or more horns. However, with one antenna the requirements were accomplished, so it was agreed with the supervisors of the project and the company to focus on a single antenna and don't design the array. Nevertheless, a brief study of the array was conducted to see if it would be worth it to develop it in future works.

2 State of the art of the technology used or applied in this thesis:

2.1 History of antennas

Around the 1830s, Faraday conducted the first experiments that addressed the coupling of electricity and magnetism and demonstrated a clear relationship. He wrapped a magnetic instrument around the galvanometer-attached wire's coils. He was essentially generating a time-varying magnetic field by rotating the magnet and based on Maxwell's equations, this magnetic field must have also had a time-varying electric field. The galvanometer, which performs the function of an antenna, detected the electromagnetic radiation that was picked up by the coil, which served as a loop antenna.

A few decades later, Heinrich Hertz used a small end-loaded dipole powered by an induction coil and a spark gap as his laboratory transmitter to perform his classical experiments. His receiver was a tiny loop, and generated sparking was used for detection. Since the resonant mean frequency of the antenna system determines the frequency produced by a spark transmitter, his 1887 experiments were carried out at Very High Frequency (VHF) and Ultra High Frequency (UHF) (60 to 500 Megahertz (MHz)), as the matching wavelengths (5.0 to 0.6 meter) were suitable for interior experimentation.

Marconi started experimenting with Hertz's apparatus in 1894. He was fascinated by the idea that by means of Hertzian waves, it might be possible to send telegraph signals, without wires, far enough for such a system to have commercial value. By 1896 he achieved a transmission distance of 2.5 kilometers using a long-wire hang-up on a kite.

Figure 2: A drawing of the kite aerial used at Signal Hill for reception of the first transatlantic wireless signal. [3]

As a result, he employed a wire antenna whose length was determined by the wavelength. The quarter wavelength monopole was utilized for the first radio link across the Atlantic Ocean.

Then he attempted transatlantic communications in 1900, employing a wire antenna

whose length was determined by the wavelength extrapolating the values used in shorter distances. In December 1901, the antenna system at Poldhu, Cornwall, broadcasted signals in the MF band (about 850 kHz).
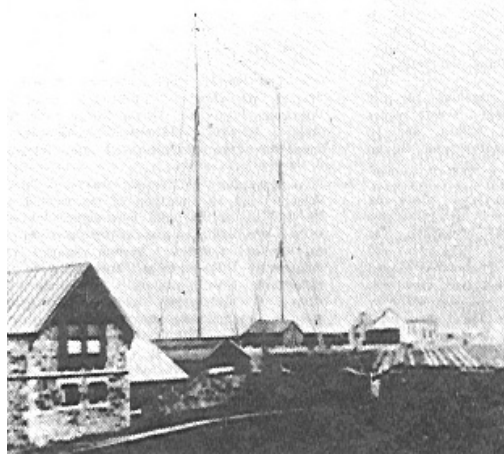
Figure 3: Quarter-wavelength dipole antenna of Marconi. [4].

2.2 Extremely high frequency motivation

The region of radio frequencies in the electromagnetic spectrum from 30 to 300 GHz is known as extremely high-frequency (EHF) by the International Telecommunication Union (ITU). It is located between the far infrared band, whose lower portion is the terahertz band, and the extremely high frequency band. It is also known as the millimeter band because the wavelengths of the radio waves in this band range from ten to one millimeter, and the term "millimeter waves" (MMW or mmWave) is frequently used to refer to this band of radiation. Indian physicist Jagadish Chandra Bose conducted the first studies of millimeter-length electromagnetic waves between 1894 and 1896, generating waves with a frequency of up to 60 GHz.

Radio waves in this band have higher atmospheric attenuation than those in lower bands because they are absorbed by atmospheric gases, as we can see in figure 4. The waves are attenuated to zero within a few meters at the top end of the band as absorption increases with frequency. Except in arid conditions, there is significant attenuation caused by atmospheric humidity, and rain (rain fade) is a serious issue even over short distances. However, compared to lower frequencies, the limited propagation range allows for shorter frequency reuse distances. The short wavelength makes it possible for antennas of average size to produce a narrow beam, further enhancing the possibility of frequency reuse. Short-range wireless networks, airport security scanners, military fire-control radar, and scientific research all make use of millimeter waves.

The newest generation of mobile phone networks, 5G networks, are using specific frequency ranges at the bottom of the band in a significant new use of millimeter waves. Because of the shorter wavelengths in this band, smaller antennas can attain the same high gain and high directivity as bigger ones in lower bands. The prospect of more effective use

Figure 4: Specific attenuation (dB/km) for atmospheric oxygen and water vapour. [11].

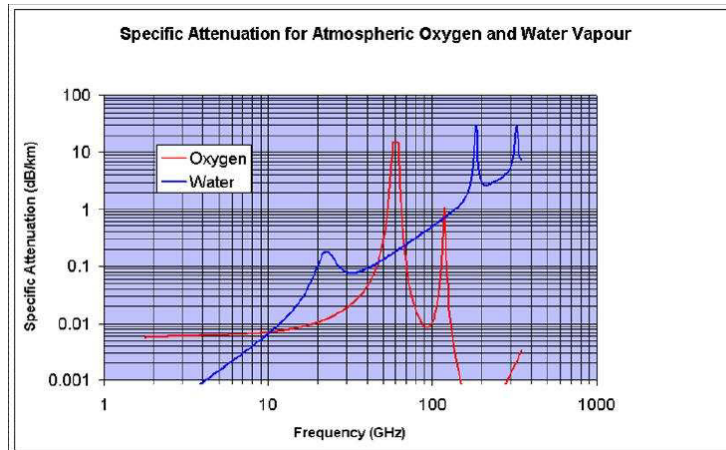of frequencies for point-to-multipoint applications is the immediate result of the high directivity and significant free space loss at these frequencies.

2.3 Automotive Radar

Automotive radar is becoming a crucial component of intelligent and autonomous features in contemporary cars, including the elimination of boring chores for drivers, a reduction in driving stress, and the addition of life-saving automatic interventions. Adaptive cruise control and automatic emergency braking, which allow a vehicle to abruptly slow down without the driver's intervention in order to avoid a potential collision, are just two of the essential safety and comfort features that have recently been made possible by the implementation of the automotive radar in many high-end cars. Due to the expensive expense of sensor technology, the usage of these functions has only been possible in high-end automobiles up until this point. In order for automotive radar technology to successfully penetrate the anticipated massive global market, both national and local regulatory bodies must collaborate with the auto industry to create relevant and harmonized standards. The penetration of vehicle radars is predicted to be around 65% in Europe and 50% in the United States by 2030.

2.4 Thesis Contribution and Overview

This thesis has presented first a really brief introduction to the history of antennas, the first wireless communications systems, and the current state of automotive radars. We have taken a special focus on the first designs of the horn antenna and the following advances that happened in the following decades. Then, it will be presented the comprehensive background of the fundamental horn antenna parameters and the theoretical analysis that should be considered in designing any Horn antenna.

Moreover, some previous works involving similar conditions and objectives will be reviewed marking the important points that were useful to move this project in the right direction.

After that, we will start getting into the design of the antenna using the software by Dassault Systemes Antenna Magus and CST. The main prototypes will be presented and the modifications between them explained, in order to transmit the knowledge obtained while developing them.

Finally, some conclusions will be drawn from both the simulation results and the overall investigation.

3 Methodology / project development:

3.1 Literature review

The horn antenna converts electromagnetic waves that are moving via a waveguide into free space. The flaring of the metal helps in the matching of the impedance of the waveguide, usually 50 Ω, to that of the free space 377Ω. A horn's wide bandwidth, low VSWR, ease of fabrication, and adjustability are its benefits.

They are made in a variety of sizes and forms to serve a wide range of practical purposes, including microwave applications, biomedical applications, directive antenna applications, communication systems, electromagnetic sensing, and as a reference source for testing other antennas. These horns can be used as feeds for various types of antennas, including compound, reflector, and lens antennas. The horn antenna can be preferred over other aperture antennas because of its wide range of uses and benefits.

In the following sections, only the fragment about horn waveguides and horn antennas of [9] is used, since it contains the theoretical background used for this particular study.

3.1.1 Introduction to Horn Antennas

There are many kinds of horn antennas. The most popular ones are the ones that can be seen in figure 5 :
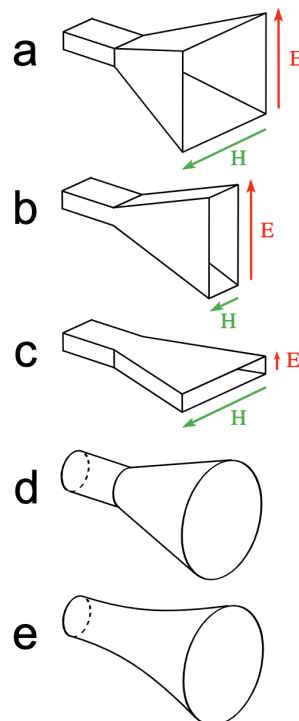

Figure 5: Common types of horn antenna [8].

a) Pyramidal horn: Four-sided pyramid-shaped horn with a rectangular cross-section. They are a typical kind that emits radio waves with linear polarization and uses rectangular waveguides.

b) A pyramidal horn with only one set of flared sides and two sets of parallel sides. In this case is flared in the direction of the waveguide's electric field, or E-field

c) Similar to the previous one but in this case, it is flared in the direction of the waveguide's magnetic field, or H-field.

d) A horn with a circular cross-section and a cone-like form. They work with cylinder-shaped waveguides.

e) A horn with curved sides in which the distance between the sides grows exponentially with length. They can have pyramidal or conical cross-sections and are also known as scalar horns. Over a broad frequency range, exponential horns have minimal internal reflections, nearly constant impedance, and other properties. They are utilized in high-performance applications like feed horns for radio telescopes and communication satellite antennas.

A waveguide can experience a variety of propagation modes. The TE10 mode, which is shown in figure 6, is the one that is most frequently employed. The waveguide's rectangular shape means that each side will have a different size. It will be assumed for the horn antenna theory and calculations that it has a width b and height a, with b < a.
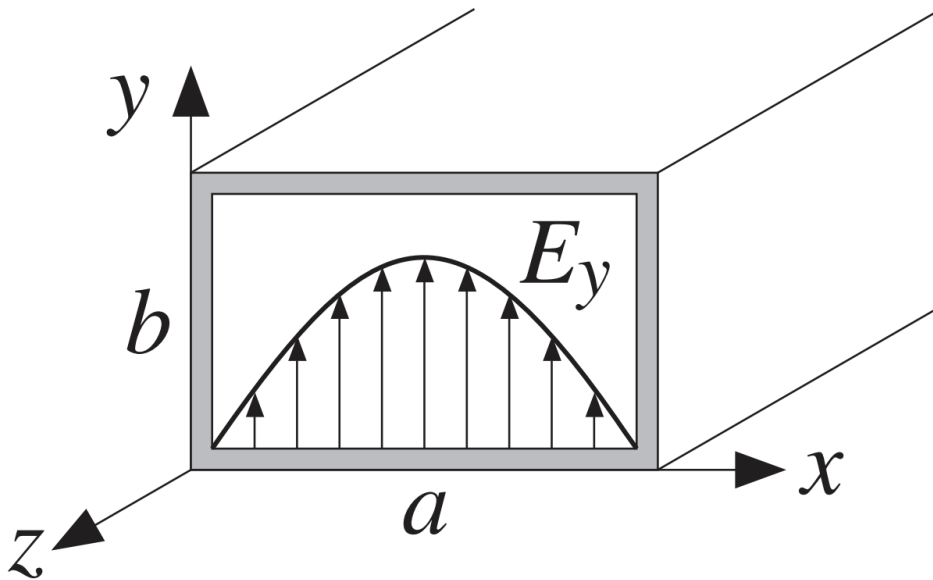

Figure 6: Example of rectangular waveguide with TE10 mode used [8].

Over an open-ended waveguide, the aperture fields are not constant. They are typically assumed to be equivalent to the fields that would be present if the guide were to be continued.

We assume that the tangential aperture fields E_a, H_a are equal to those of the TE_{10} mode by placing the origin in the center of the aperture. Then we obtain:

$$E_y(x') = E_0 \cos\left(\frac{\pi x'}{a}\right), \quad H_x(x') = -\frac{1}{\eta_{TE}} E_0 \cos\left(\frac{\pi x'}{a}\right) \tag{1}$$

where $\eta_{TE} = \eta/K$ with η being the antenna efficiency and $K = \sqrt{1 - \omega_c^2/\omega^2} = \sqrt{1 - (\lambda/2a)^2}$.

Since we will work with smaller apertures, such as $0.5\lambda \leq a \leq 2\lambda$, the generalized Huygens source condition can be used. The radiated fields are:

$$E_\theta = jk\frac{e^{-jkr}}{2\pi r} c_\theta f_y(\theta,\phi) \sin\phi \tag{2}$$

$$E_\phi = jk\frac{e^{-jkr}}{2\pi r} c_\phi f_y(\theta,\phi) \cos\phi \tag{3}$$

where $f_y(\theta,\phi)$ is the aperture Fourier transform of $E_y(x')$. After some manipulation detailed in [9] it follows that:

$$f_y(\theta,\phi) = E_0 \frac{2ab}{\pi} \frac{\cos(\pi v_x)}{1 - 4v_x^2} \frac{\sin(\pi v_y)}{\pi v_y}$$

where $\nu_x = k_x a/2\pi$ and $\nu_y = k_y b/2\pi$, or,

$$v_x = \frac{a}{\lambda} \sin\theta \cos\phi, \quad v_y = \frac{b}{\lambda} \sin\theta \sin\phi$$

If the aperture is terminated in a ground plane, the PEC case should be selected as the obliquity factor. If the aperture is radiating into space, the ordinary Huygens source case should be selected. If not, the modified Huygens source case should be selected. Thus,

$$\begin{bmatrix} c_\theta \\ c_\phi \end{bmatrix} = \begin{bmatrix} 1 \\ \cos\theta \end{bmatrix}, \quad \frac{1}{2}\begin{bmatrix} 1 + \cos\theta \\ 1 + \cos\theta \end{bmatrix}, \quad \frac{1}{2}\begin{bmatrix} 1 + K\cos\theta \\ K + \cos\theta \end{bmatrix}$$

By normalizing all three cases to unity at $\theta = 0°$, we may combine them into:

$$c_E(\theta) = \frac{1 + K\cos\theta}{1 + K}, \quad c_H(\theta) = \frac{K + \cos\theta}{1 + K}$$

where K is one of the three possible values:

$$K = 0, \quad K = 1, \quad K = \frac{\eta}{\eta_{TE}} = \sqrt{1 - \left(\frac{\lambda}{2a}\right)^2}$$

The following equations show the normalized gains along the two main planes. For the xz - or the H-plane, we set $\phi = 0°$, which gives $E_\theta = 0$:

$$g_H(\theta) = \frac{|E_\phi(\theta)|^2}{|E_\phi|_{\max}^2} = |c_H(\theta)|^2 \left|\frac{\cos(\pi v_x)}{1 - 4v_x^2}\right|^2, \quad v_x = \frac{a}{\lambda}\sin\theta$$

And, for the yz - or E-plane, we set $\phi = 90°$, which gives $E_\phi = 0$:

$$g_E(\theta) = \frac{|E_\theta(\theta)|^2}{|E_\theta|^2_{\max}} = |c_E(\theta)|^2 \left| \frac{\sin(\pi v_y)}{\pi v_y} \right|^2, \quad v_y = \frac{b}{\lambda} \sin \theta$$

The expression for the waveguide aperture's gain and directivity is then obtained. The highest level of intensity occurs at $\theta = 0°$. Because $c_\theta(0) = c_\phi(0)$, we have:

$$U_{\max} = \frac{1}{2\eta} |\boldsymbol{E}(0, \phi)|^2 = \frac{1}{2\lambda^2 \eta} c^2_\theta(0) |f_y(0, \phi)|^2 = \frac{1}{2\lambda^2 \eta} c^2_\theta(0) |E_0|^2 \frac{4(ab)^2}{\pi^2}$$

The power propagated down the waveguide, as determined by the following equation, is the total power that passes through the aperture and is radiated.

$$P_{\mathrm{rad}} = \frac{1}{4\eta_{TE}} |E_0|^2 ab$$

The gain or directivity of the aperture will be:

$$G = 4\pi \frac{U_{\max}}{P_{\mathrm{rad}}} = \frac{4\pi}{\lambda^2} \frac{8}{\pi^2} (ab) \frac{\eta_{TE}}{\eta} c^2_\theta(0)$$

For the PEC and ordinary Huygens cases, $c_\theta(0) = 1$. Assuming $\eta_{TE} \simeq \eta$:

$$G = \frac{4\pi}{\lambda^2} \frac{8}{\pi^2} (ab) = 0.81 \frac{4\pi}{\lambda^2} (ab)$$

As a result, the waveguide aperture's effective area is $A_{\mathrm{eff}} = 0.81(ab)$ and its aperture efficiency is $e = 0.81$. For the modified Huygens case, we have for the obliquity factor $c_\theta(0) = (K + 1)/2$ with $K = \eta/\eta_{TE}$. It follows that:

$$G = \frac{4\pi}{\lambda^2} \frac{8}{\pi^2} (ab) \frac{(K+1)^2}{4K}$$

For waveguides larger than about a wavelength, the directivity factor $(K + 1)^2/4K$ is practically equal to unity.

3.1.2 Fields and geometrical parameters of Horn antennas

First of all, it is quite possible to leave a waveguide open and let signal radiate from this. However, this is not particularly efficient. Signals passing along the waveguide see a sudden transition from the waveguide to free space which has an impedance of around 377Ω.

The result of this sudden transition is to cause signals to be reflected back along the waveguide as standing waves - theory shows that this is exactly the same as for poor matches at the end of coaxial or other forms of wire-based transmission lines.

The waveguide can be flared or tapered out to get around this problem. As a result, there is a smooth transition from the waveguide's impedance to that of free space. It functions

in a manner similar to a progressive matching transformer. The flare acts similarly to an optical medium with a smoothly fluctuating refractive index or a tapered transmission line. Additionally, the horn's large aperture projects the waves as a narrow beam.

The exponential horn is the sort of horn that offers the best match. Pyramidal or conical horns, on the other hand, provide an adequate match for the majority of applications and are simpler and less expensive to manufacture. Because in this project a pyramidal horn is the one used, that is the one we will discuss from now on.
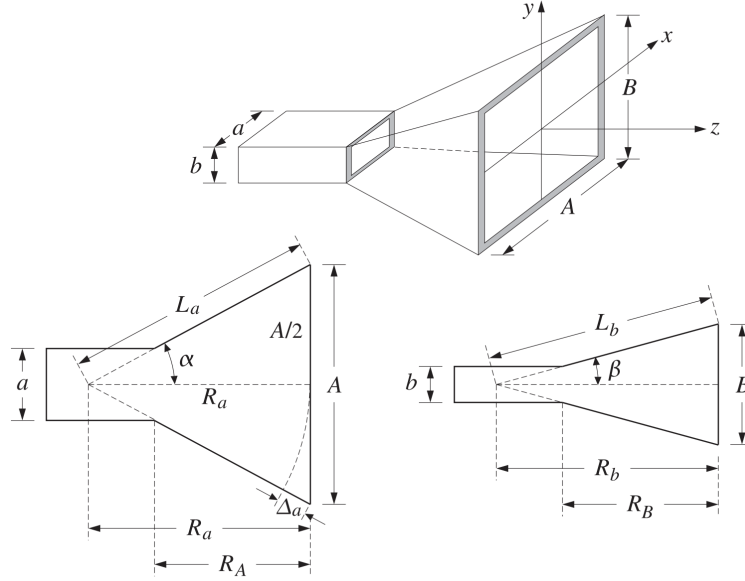

Figure 7: Geometry of a pyramidal horn. [9].

In the previous figure, we can observe the parameters used in [9] to define horn antennas, being

$$\Delta_a(x) = \frac{x^2}{2R_a}, \quad \Delta_b(y) = \frac{y^2}{2R_b}$$

The relative phase differences at the point (x, y) on the horn's aperture in relation to the aperture's center are represented by the quantities $k\Delta_a(x)$ and $k\Delta_b(y)$. The aperture electric field is considered to have the following structure to account for these phase differences:

$$E_y(x, y) = E_0 \cos\left(\frac{\pi x}{A}\right) e^{-jk\Delta_a(x)} e^{-jk\Delta_b(y)}, \text{ then,}$$
$$E_y(x, y) = E_0 \cos\left(\frac{\pi x}{A}\right) e^{-jkx^2/2R_a} e^{-jky^2/2R_b} \tag{4}$$

We observe that the electric field is $E_y(x, y) = E_0 \cos(\pi x/a)$ at the waveguide's connecting end and progressively transforms into Equation 4 at the horn end.

The Huygens source assumption is quite correct for the tangential aperture magnetic field, $Hx(x, y) = -Ey(x, y)/eta$, because the aperture sides A, B are assumed to be larger than $lambda$, so that:

$$H_x(x,y) = -\frac{1}{\eta}E_0 \cos\left(\frac{\pi x}{A}\right) e^{-jkx^2/2R_a}e^{-jky^2/2R_b}$$

The maximum phase deviations in radians are represented by the numbers $k\Delta_a$ and $k\Delta_b$. As a result, the greatest variances in cycles will be Δ_a/λ and Δ_b/λ. The following is then defined:

$$S_a = \frac{\Delta_a}{\lambda} = \frac{A^2}{8\lambda R_a}, \quad S_b = \frac{\Delta_b}{\lambda} = \frac{B^2}{8\lambda R_b}$$

It turns out that $S_a = 3/8$ and $S_b = 1/4$ are roughly the best values for these parameters that produce the most directivity. These numbers will be used later in the creation of the ideal horns. We define the relevant parameters in order to derive practical formulas for the horn's radiation patterns:

$$\sigma_a^2 = 4S_a = \frac{A^2}{2\lambda R_a}, \quad \sigma_b^2 = 4S_b = \frac{B^2}{2\lambda R_b}$$

These constants' near-optimal values are $\sigma_a = \sqrt{4S_a} = \sqrt{4(3/8)} = 1.2247$ and $\sigma_b = \sqrt{4S_b} = \sqrt{4(1/4)} = 1$. However, the true optimum values would be $\sigma_a = 1.2593$ and $\sigma_b = 1.0246$.

Then, $k = 2\pi/\lambda$ and $2\lambda R_a = A^2/\sigma_a^2$ and $2\lambda R_b = B^2/\sigma_b^2$ is replaced in Equation 4, in order to rewrite the aperture fields in the form:

$$E_y(x,y) = E_0 \cos\left(\frac{\pi x}{A}\right) e^{-j(\pi/2)\sigma_a^2(2x/A)^2}e^{-j(\pi/2)\sigma_b^2(2y/B)^2}$$

$$H_x(x,y) = -\frac{1}{\eta}E_0 \cos\left(\frac{\pi x}{A}\right) e^{-j(\pi/2)\sigma_a^2(2x/A)^2}e^{-j(\pi/2)\sigma_b^2(2y/B)^2}$$

For $-A/2 \le x \le A/2$ and $-B/2 \le y \le B/2$.

3.1.3 Radiation fields

Similar to the open-ended waveguide, the electric field's aperture Fourier transform only has a y-component, which is represented by:

$$f_y(\theta,\phi) = \int_{-A/2}^{A/2}\int_{-B/2}^{B/2} E_y(x,y)e^{jk_x x + jk_y y}dxdy$$

$$= E_0 \int_{-A/2}^{A/2} \cos\left(\frac{\pi x}{A}\right) e^{jk_x x}e^{-j(\pi/2)\sigma_a^2(2x/A)^2}dx \cdot \int_{-B/2}^{B/2} e^{jk_y y}e^{-j(\pi/2)\sigma_b^2(2y/B)^2}dy$$

The following diffraction-like integrals can be used to express the aforementioned integrals:

$$F_0(\nu,\sigma) = \int_{-1}^{1} e^{j\pi\nu\xi}e^{-j(\pi/2)\sigma^2\xi^2}d\xi \tag{5}$$

$$F_1(\nu, \sigma) = \int_{-1}^{1} \cos\left(\frac{\pi\xi}{2}\right) e^{j\pi\nu\xi} e^{-j(\pi/2)\sigma^2\xi^2} d\xi \tag{6}$$

$F_0(\nu, \sigma)$ can be expressed as:

$$F_0(\nu, \sigma) = \frac{1}{\sigma} e^{j(\pi/2)(v^2/\sigma^2)} \left[F\left(\frac{\nu}{\sigma} + \sigma\right) - F\left(\frac{\nu}{\sigma} - \sigma\right)\right]$$

where $F(x) = C(x) - jS(x)$ is the standard Fresnel integral. Following that, the function $F_1(\nu, \sigma)$ can be written as $F_0(\nu, \sigma)$:

$$F_1(\nu, \sigma) = \frac{1}{2}\left[F_0(\nu + 0.5, \sigma) + F_0(\nu - 0.5, \sigma)\right]$$

Next, the radiation patterns are expressed in terms of the functions 5 and 6. Defining the normalized wavenumbers $\nu_x = k_x A/2\pi$ and $\nu_y = k_y B/2\pi$, we have:

$$\nu_x = \frac{A}{\lambda}\sin\theta\cos\phi, \quad v_y = \frac{B}{\lambda}\sin\theta\sin\phi$$

When variables are changed to $\xi = 2y/B$, the y-integral can be expressed in terms of $F_0(\nu, \sigma)$ as follows:

$$\int_{-B/2}^{B/2} e^{jk_y y} e^{-j(\pi/2)\sigma_b^2(2y/B)^2} dy = \frac{B}{2}\int_{-1}^{1} e^{j\pi v_y\xi} e^{-j(\pi/2)\sigma_b^2\xi^2} d\xi = \frac{B}{2}F_0\left(v_y, \sigma_b\right)$$

When we switch the variables to $\xi = 2x/A$, we discover the following for the x-integral:

$$\int_{-A/2}^{A/2} \cos\left(\frac{\pi x}{A}\right) e^{jk_x x} e^{-j(\pi/2)\sigma_a^2(2x/A)^2} dx$$

$$= \frac{A}{2}\int_{-1}^{1} \cos\left(\frac{\pi\xi}{2}\right) e^{j\pi v\xi} e^{-j(\pi/2)\sigma_a^2\xi^2} d\xi = \frac{A}{2}F_1\left(\nu_x, \sigma_a\right)$$

The Fourier transform $f_y(\theta, \phi)$ will then be:

$$f_y(\theta, \phi) = E_0\frac{AB}{4}F_1\left(v_x, \sigma_a\right)F_0\left(v_y, \sigma_b\right)$$

As limiting cases of the previous equation, the open-ended waveguide and the sectoral horns can be considered as follows:

1. An open-ended waveguide with: $\quad \sigma_a = 0, \quad A = a, \quad \sigma_b = 0, \quad B = b$

2. Sectoral horn for the H-plane: $\quad \sigma_a > 0, \quad A > a, \quad \sigma_b = 0, \quad B = b$

3. Sectoral horn for the E-plane: $\quad \sigma_a = 0, \quad A = a, \quad \sigma_b > 0, \quad B > b$

In these circumstances, the following simplified forms can be used to replace the F-factors with $\sigma = 0$:

$$F_0\left(v_y, 0\right) = 2\frac{\sin\left(\pi v_y\right)}{\pi v_y}, \quad F_1\left(v_x, 0\right) = \frac{4}{\pi}\frac{\cos\left(\pi v_x\right)}{1 - 4v_x^2}$$

At this point, the fields from Huygens source are used, where all points at the aperture are related by the uniform plane-wave relationship $\boldsymbol{H}_a = \frac{1}{\eta}\hat{\mathbf{n}} \times \boldsymbol{E}_a$ with obliquity factors $c_\theta(\theta) = c_\phi(\theta) = (1 + \cos\theta)/2$.

$$E_\theta = jk\frac{e^{-jkr}}{2\pi r}c_\theta\left[f_x\cos\phi + f_y\sin\phi\right]$$
$$E_\phi = jk\frac{e^{-jkr}}{2\pi r}c_\phi\left[f_y\cos\phi - f_x\sin\phi\right]$$

Replacing $k = 2\pi/\lambda$, we can obtain the following expressions:

$$E_\theta = j\frac{e^{-jkr}}{\lambda r}c_\theta(\theta)f_y(\theta, \phi)\sin\phi$$
$$E_\phi = j\frac{e^{-jkr}}{\lambda r}c_\phi(\theta)f_y(\theta, \phi)\cos\phi$$

or, explicitly,

$$E_\theta = j\frac{e^{-jkr}}{\lambda r}E_0\frac{AB}{4}\left(\frac{1 + \cos\theta}{2}\right)\sin\phi F_1\left(v_x, \sigma_a\right)F_0\left(\nu_y, \sigma_b\right)$$
$$E_\phi = j\frac{e^{-jkr}}{\lambda r}E_0\frac{AB}{4}\left(\frac{1 + \cos\theta}{2}\right)\cos\phi F_1\left(v_x, \sigma_a\right)F_0\left(v_y, \sigma_b\right)$$

The main conclusion that can be extracted from these results is that the beamwidth in the two planes can be controlled by aperture dimensions almost independently.

3.1.4 Directivity

The Poynting vector of the aperture fields over the horn region is integrated to get the radiated power P_{rad}. Thus,

$$P_{\text{rad}} = \frac{1}{4\eta}\left|E_0\right|^2\left(AB\right)$$

As a result, the horn's directivity will be as follows:

$$G = 4\pi\frac{U_{\text{max}}}{P_{\text{rad}}} = \frac{4\pi}{\lambda^2}(AB)\frac{1}{8}\left|F_1\left(0, \sigma_a\right)F_0\left(0, \sigma_b\right)\right|^2 = e\frac{4\pi}{\lambda^2}AB$$

where we defined the aperture efficiency e by:

$$e\left(\sigma_a, \sigma_b\right) = \frac{1}{8}\left|F_1\left(0, \sigma_a\right)F_0\left(0, \sigma_b\right)\right|^2$$

then the optimum horn directivity can be obtained:

$$G = 0.49 \frac{4\pi}{\lambda^2} AB$$

In this case, "optimum" means maximizing the gain given the geometrical constraints of the horn.

3.1.5 Design

Finding the sides A and B that produce a certain gain G, meet the requirement $R_A = R_B$, and fit geometrically into a given waveguide with sides a and b is difficult when designing a horn antenna.

The two design equations for A, B are the following equations:

$$G = e \frac{4\pi}{\lambda^2} AB, \quad \frac{\sigma_b^2}{\sigma_a^2} = \frac{B(B-b)}{A(A-a)} \tag{7}$$

The constant aspect ratio enclosure gets simplified since the second condition is already met because $\sigma_b = r\sigma_a$. After that, the first condition for A can be solved, yielding $B = rA$ and $R_A = A(A-a)/\left(2\lambda\sigma_a^2\right)$:

$$G = e \frac{4\pi}{\lambda^2} A(rA) \Rightarrow A = \lambda \sqrt{\frac{G}{4\pi e r}}$$

One must find the two unknowns A, B in the system of equations 7 for uneven aspect ratios and arbitrary σ_a, σ_b. The second equation in 7 can be solved for B in terms of $A, a, and b$, avoiding negative solutions for B and substituting the previous system with:

$$f_1(A, B) \equiv B - \left[\frac{b}{2} + \sqrt{\frac{b^2}{4} + \frac{\sigma_b^2}{\sigma_a^2} A(A-a)} \right] = 0$$

$$f_2(A, B) \equiv AB - \frac{\lambda^2 G}{4\pi e} = 0$$

Newton's technique can be used to solve this system iteratively, which entails starting with some initial values A, B and repeatedly replacing them with the corrected values $A + \Delta A$ and $B + \Delta B$. The corrections are calculated from:

$$\begin{bmatrix} \Delta A \\ \Delta B \end{bmatrix} = -\mathcal{M}^{-1} \begin{bmatrix} f_1 \\ f_2 \end{bmatrix}, \text{ where } \mathcal{M} = \begin{bmatrix} \partial_A f_1 & \partial_B f_1 \\ \partial_A f_2 & \partial_B f_2 \end{bmatrix}$$

Where the matrix $\mathcal{M}$ is equal to:

$$\mathcal{M} = \begin{bmatrix} -\frac{\sigma_b^2}{\sigma_a^2} \frac{2A-a}{(2B-b-2f_1)} & 1 \\ B & A \end{bmatrix} \simeq \begin{bmatrix} -\frac{\sigma_b^2}{\sigma_a^2} \frac{2A-a}{2B-b} & 1 \\ B & A \end{bmatrix}$$

where the term $2f_1$ was replaced by zero (this is approximately correct near convergence.) Assuming that A, B will be significantly larger than a, b will yield good initial values. Then, equation 7 can be roughly expressed as follows:

$$G = e\frac{4\pi}{\lambda^2}AB, \quad \frac{\sigma_b^2}{\sigma_a^2} = \frac{B^2}{A^2}$$

The system can be easily solved giving:

$$A_0 = \lambda\sqrt{\frac{G}{4\pi e}\frac{\sigma_a}{\sigma_b}}, \quad B_0 = \lambda\sqrt{\frac{G}{4\pi e}\frac{\sigma_b}{\sigma_a}}$$

3.2 First steps

The first steps regarding the design of the antenna were taken on Antenna Magus, which provided a first prototype. This first prototype didn't accomplish the main requirements that were set. However, it gave an idea of the dimensions that the antenna should have.

First of all, and for simplicity, from this point on we will use the simplified notation used by the Antenna Magus software, which can be seen in figure 8.
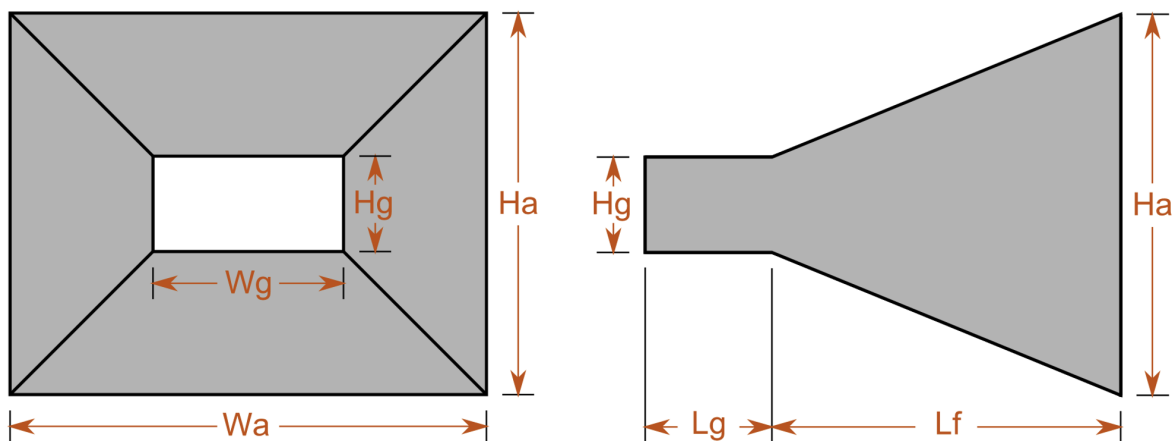

Figure 8: Geometry of a pyramidal horn in Antenna Magus. [9].

Those six parameters will be the initial values by which the antenna was defined since the first model was obtained using the Antenna Magus software. As we can see in figure 9 we can quickly create a design using the already-existent template of a pyramidal Horn antenna.

Indicating then the required frequency and Field of View (FOV) goals in the interface of figure 10.

The results obtained are obviously far from the requirements of the project. However, it is a good starting point to get an idea of the dimensions that the antenna will have, in the order of a few millimeters. As we can see in figure 11 the initial antenna generated by the software will need a lot of work done in order to accomplish the requirements of the antenna.
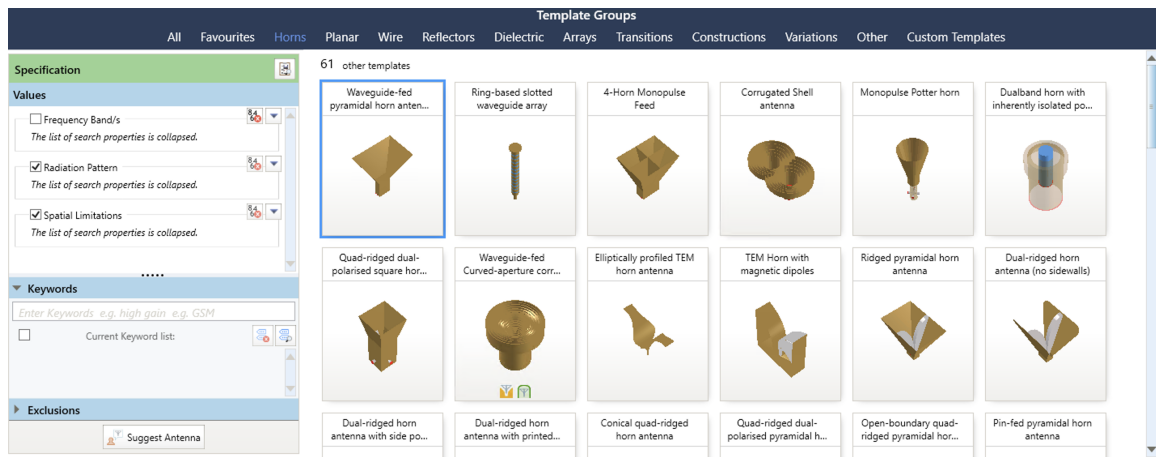
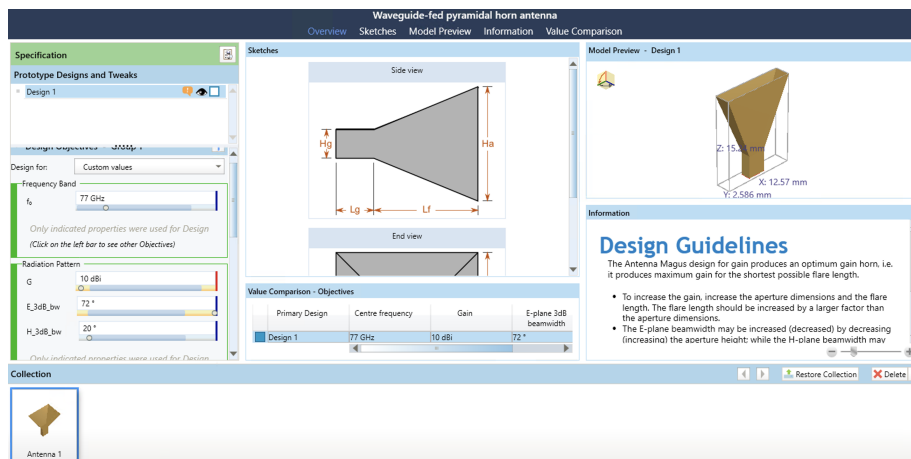Figure 9: Antenna Magus templates. [9].

Figure 10: Antenna Magus user interface to define the antenna. [9].

From this point on the objective will be to modify the antenna to accomplish the required FOV and the matching is below -15 dB.

Parameter	Value
Width of waveguide section	3.056 mm
Height of waveguide section	1.528 mm
Length of waveguide section	3.893 mm
Aperture width	12.57 mm
Aperture height	2.586 mm
Aperture length	11.35 mm

3.3   Becoming familiar with CST

Even though it was the first time I used Antenna Magus, it didn't take long for me to get familiar with it and get the results I wanted. This is because the software is really
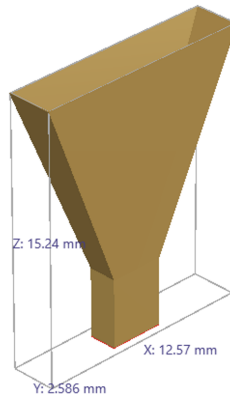
Figure 11: Initial antenna obtained. [9].

intuitive and user-friendly, so just looking a little bit through the interface of the program you can start using it right after.

Moreover, as was explained in the previous chapter, the expected results were only a general starting point to get an idea of the dimensions of the antenna. This means that the amount of tuning and optimization did in Antenna Magus was very little and didn't bring that much trouble.

On the other hand, CST Studio Suite was from the very beginning more challenging since it has a much wider range of possibilities. This is obviously a positive thing in the long run, but at the start can be a little bit overwhelming.

3.4   Design decisions

One of the first decisions made was to use the same parameters from Antenna Magus to define the antenna. This could seem like a trivial decision, but as we can see in figure 7 the flare angles α and β in both axis can be used to define the antenna. However, with the objective to make the creation of the antenna in the CST environment straightforward, the length of the aperture will be used, which is obviously related to angles α and β with a simple trigonometric identity but working with our three parameters of the aperture similar results can be obtained.

The next step was to decide which material and what thickness to use. The first one was pretty easy and didn't change throughout the whole project, Perfect Electric Conductor (PEC). Nonetheless, the thickness of the waveguide and the aperture were conditioned by the fact that this antenna is supposed to be created in reality. As we have seen, at Extremely High Frequency (EHF) the measures of the antenna will be in the order of a few millimeters. To create an antenna that small with precision special machinery is required. That machinery has mechanical boundaries that will ultimately condition the design. In the beginning and since those boundaries were unknown still, a thickness of 0.1 mm was used for the first prototypes. Later on, it was changed to 0.5 mm, which affected

the antenna adaptation bringing the S11 parameter again far from our objective and a new optimization was needed.

Finally, in order to obtain reliable simulation results while reducing the time to obtain them some changes were supposed to be made. Those changes were done after some weeks of work with the invaluable help of professor Pavel Hazdra. The main changes can be seen in the following figures.

Figure 12 and figure 13 show the boundaries and symmetries used in order to create appropriate conditions for the simulations while having a reasonable simulation time. On the boundaries aspect, due to the fact that a computer is only capable of calculating problems that have a finite expansion, you need to specify the boundary conditions. This can be done within this dialog box. When you enter the boundaries property sheet, the modeled structure is displayed with a surrounding bounding box colored with regard to the boundary condition at each boundary. In our case, we are going to use "Open (add space)", which operates like free space: waves can pass this boundary with minimal reflections. Moreover, it adds some extra space for far-field calculation. On the other hand, we will take advantage of the fact that the antenna will be symmetric in both axis of the aperture to indicate the program to calculate only the results in one of the quadrants by this dialog box.
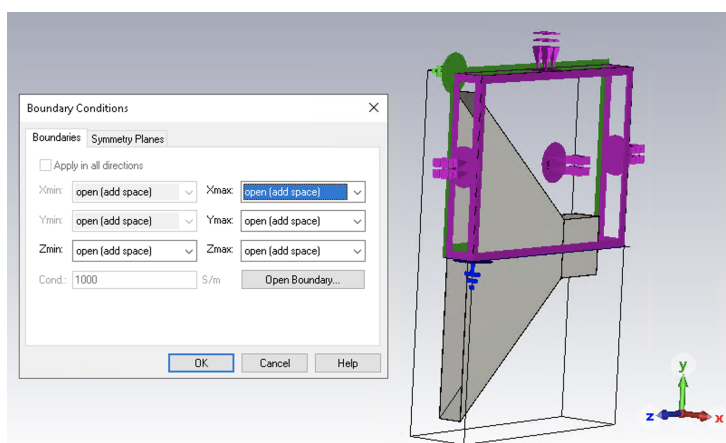

Figure 12: Boundaries defined.

After we have set up our model geometrically and assigned the appropriate power sources and boundary conditions, our model has to be translated into a representation that is suitable for the simulation. For general-purpose EM simulation methods, the calculation domain has to be subdivided into small cells, on which Maxwell's Equations are to be solved.

CST Studio Suite offers a variety of meshes and mesh generation algorithms, with the easy possibility of cross-verifying different methods and meshes in the same GUI. The mesh influences the accuracy and speed of your simulation. In our case, we will use the hexahedral mesh as we can see in figure 14.

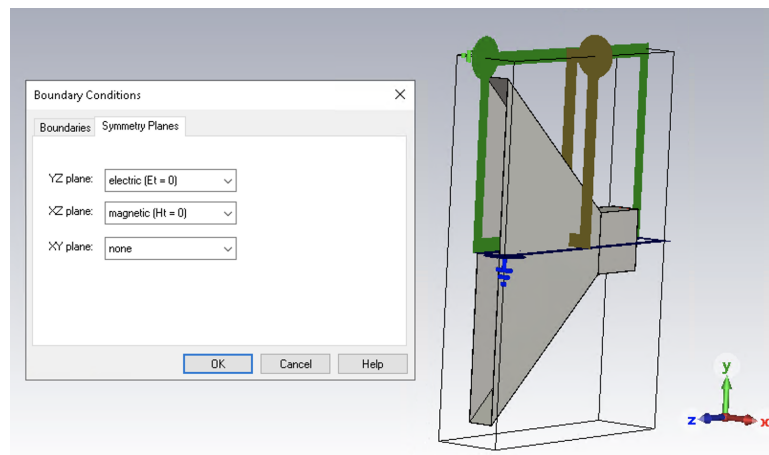The monitor dialog box gives us the opportunity to define field monitors that we might
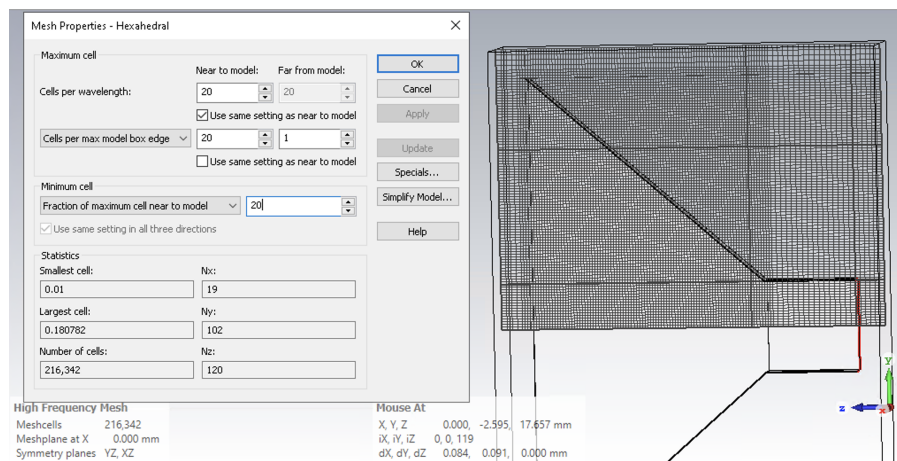
Figure 13: Symmetries defined.

Figure 14: Mesh defined.

need to obtain additional information on the electromagnetic field distribution inside our structure. It is possible to define frequency as well as time monitors. After a calculation, we will be able to observe our field monitors by selecting them in the Navigation Tree. In our case, we will use the "Farfield/RCS" option with frequencies between 76 GHz and 80 GHz.

Moreover, a time domain solver calculates the development of fields through time at discrete locations and at discrete time samples. It calculates the transmission of energy between various ports or other excitation sources and/or open space of the investigated structure. In our case, we will use a Hexahedral mesh with a -40 dB accuracy.

Finally, we can see some tables in the Navigation Tree defined to see better the results obtained. In figure 15 we can see all the ones that were defined and in figure 16 we can observe the one referred to as the S11 parameter.
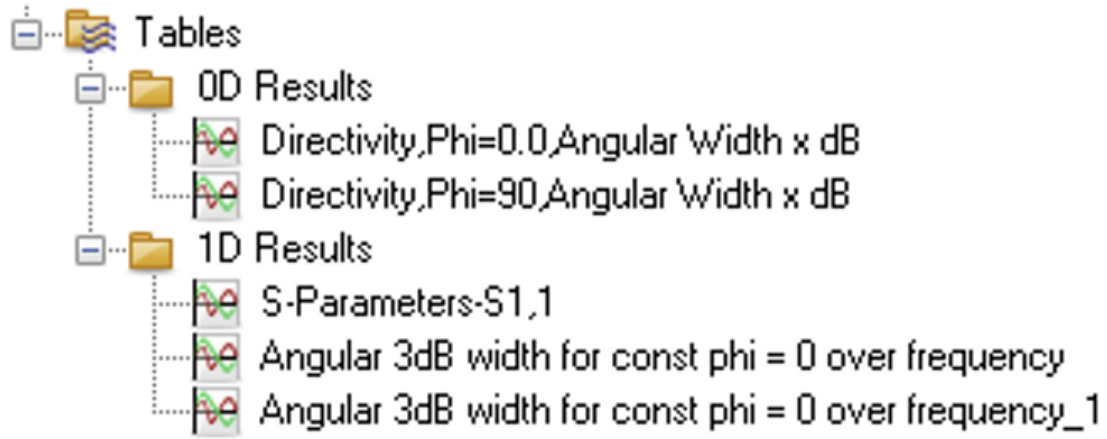
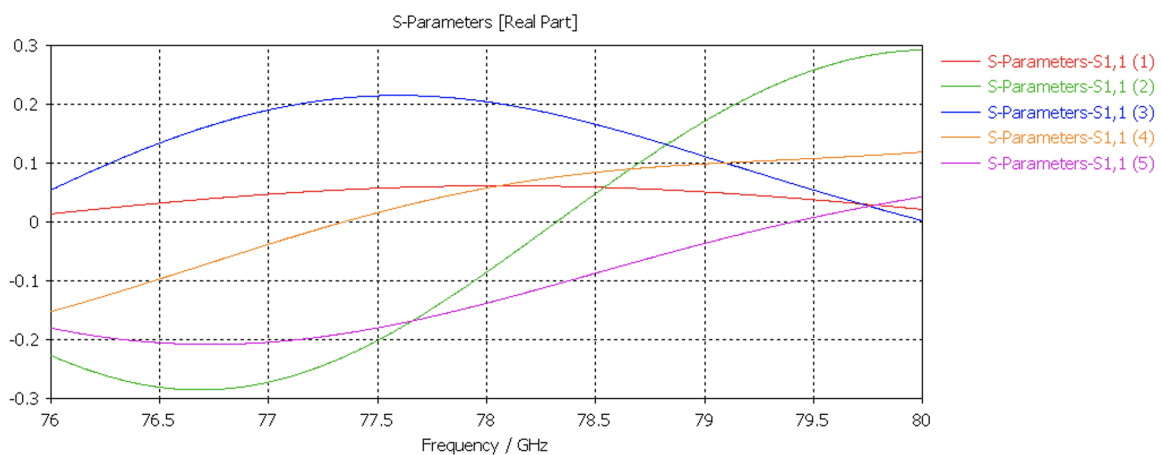Figure 15: Tables used to see clearly the results.

Figure 16: Example of Table used for the S11 parameter.

4 Results

After becoming familiar with the CST software and obtaining the first antenna prototype in Antenna Magus the experimental stage of the project can be divided into four blocks:

- Phase 1: Focused on obtaining the required field of view.

- Phase 2: Focused on adapting the antenna.

- Phase 3: Focused on optimizing the antenna again after increasing the thickness.

- Phase 4: Focused on simulating a few horn arrays and evaluating if it would be worth it to pursue this idea.

4.1 First phase

After becoming a little bit familiar with the program we could start the first simulations. In table 1 we can observe the first antenna prototype parameters. Those are the antenna designs that were discussed in order to pave a path forward, defining the changes needed and the next main objectives.

Parameter	P1	P2	P3	P4	P5
Width of waveguide section (mm)	3.08906	3.15	3.15	3.45	3.0988
Height of waveguide section (mm)	1.6599	1.285	1.689	1.33479	1.5494
Length of waveguide section (mm)	3.58193	3.55	3.551	3.08073	3.0988
Aperture width (mm)	12.2167	15.55	14.4	17.069	17.069
Aperture height (mm)	3.58801	1.285	1.7	1.37088	1.37088
Aperture length (mm)	12.4968	13.92	12.5	8.21678	8.027

Table 1: First five prototypes parameters

Those first five prototypes were developed over several weeks and lots of simulations. Part of the designing process difficulty was knowing what to optimize first. At the very beginning, the prototypes tried to find a balance between a good FOV and a reasonable gain. However, it was clear after a few days that focusing on gain was not the right move. Instead, the first objective was trying to find the right dimensions for the Aperture height and width so the FOV meets the requirements. Nevertheless, it was unknown if the initial values obtained by Antenna Magus would be able to achieve the required FOV by optimizing them.

The general idea is to increase the height of the aperture to obtain a narrower beam in elevation cut or reduce it to obtain a wider beam. The same happens in the azimuth cut, but this time modifying the aperture width. After several parameter sweeps and optimizations, it was clear that just by changing the aperture height and width we wouldn't meet the requirements imposed. For that reason, in Prototype 4, the length of the antenna aperture started to be iterated too to find a new set of values. After several simulations, it was clear that the best range of values would be around 8 mm and 9 mm since the FOV and the adaptation were reasonably good.
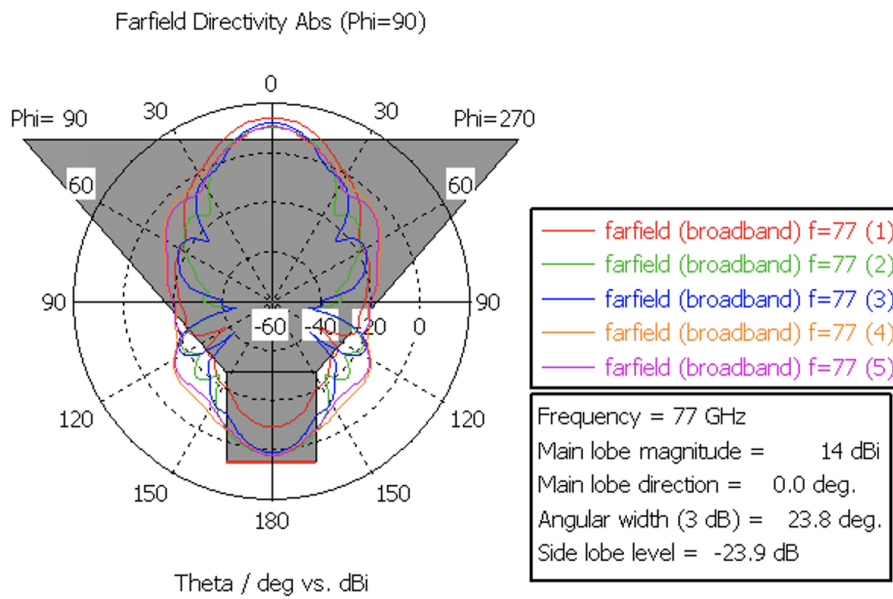
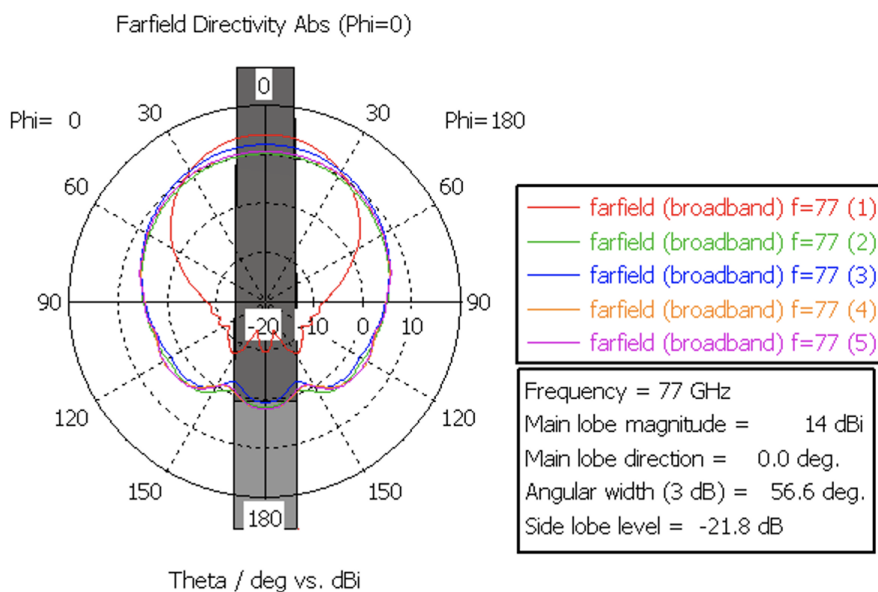Figure 17: Elevation plane obtained from prototypes 1 to 5.

Figure 18: Azimuth cut obtained from prototypes 1 to 5.

As we can see in figures 17 and 18 the changes in the FOV after Prototype 1, which was basically a replica of the model obtained in Antenna Magus (Prototype 0) but with better gain, always tried to be as close as possible to the FOV objective but trying different sets of parameter values. Besides, always taking into account the obtained S11 parameter, optimizing the parameters a little bit to improve it as much as possible. This process really never stop, since the possibility of using a range of values that would ultimately lead to a dead end was always there, and having other sets of values gave us always an

alternative to investigate. Moreover, as we can see from Prototype 4 to Prototype 5 the width and the height of the waveguide were both changed at the same time to match the standardized measures of the WR12 waveguide of the Electronic Industries Alliance (EIA) standard, also known as R740 at the International Electrotechnical Commission (IEC). This change didn't affect the FOV results but the adaptation got worse.
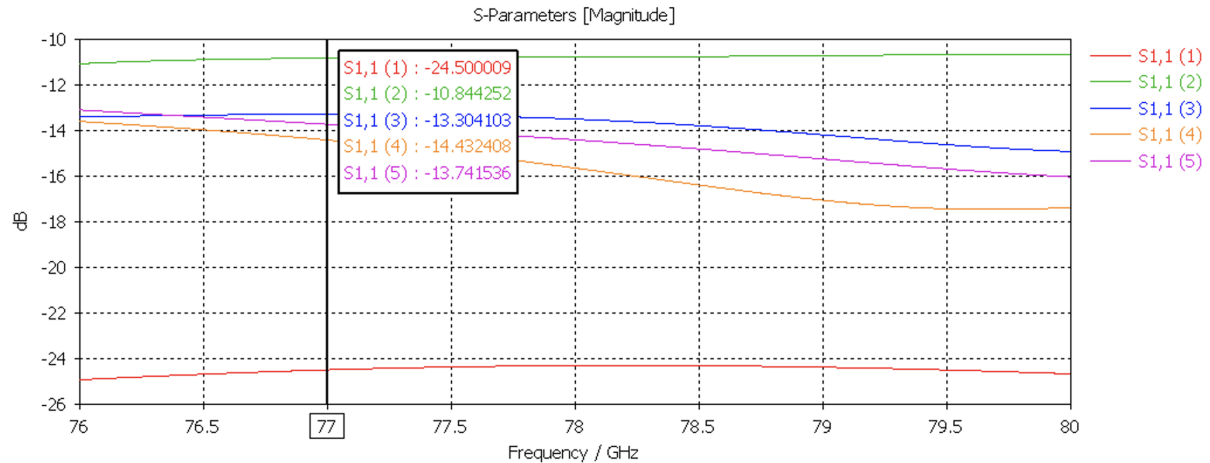

Figure 19: S11 parameters obtained from prototypes 1 to 5.

As we can see in 19, from Prototype 2 forward the S11 parameter improved, but with the change in the waveguide parameters it fell slightly. As it has been said, these results were the best ones obtained after several optimizations within the range of values displayed in table 1 for each prototype. The adaptation of the S11 parameter was supposed to be done by modifying the aperture length. In changes in the order of millimeters, the effect in the adaptation was noticeable and it was one of the factors taken into account when selecting a new set of values to try. However, these changes also affected the FOV, so when adapting the antenna big changes in the length took the design back to the starting point. Finding a balance between all those values was key to determining a good design. After discussing with the supervisor it was determined that the S11 parameter was not possible to improve. For that reason, several ideas were explored to improve it as much as possible.

4.2 Second phase

During this second phase, the main focus was going to be adapting the antenna in order to obtain a S11 parameter below -15 dB. There were different techniques discussed to do so. The first one was to use a different kind of feeding with a coaxial cable that would look like in figure 20.

Using this kind of feeding we would be able to parameterize the position of the coaxial cable in the waveguide and observe how would that affect the results regarding the S11 parameter.

It was also an interesting choice to use a stepped waveguide parameterizing the different

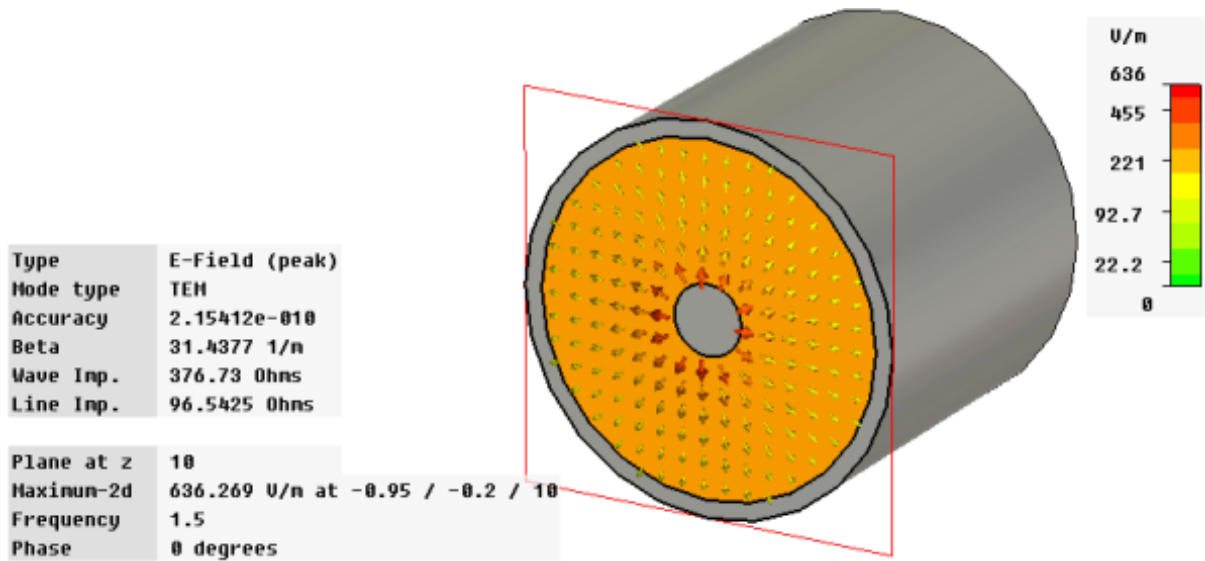|	
Type	E-Field (peak)
Mode type	TEM
Accuracy	2.15412e-010
Beta	31.4377 1/m
Wave Imp.	376.73 Ohms
Line Imp.	96.5425 Ohms
Plane at z	10
Maximum-2d	636.269 V/m at -0.95 / -0.2 / 10
Frequency	1.5
Phase	0 degrees

Figure 20: Coaxial cable created in CST.

[12]

levels of the waveguide since some papers indicated that they successfully adapted their horn antenna using this approach. Figure 21 is an example of the geometry of a rectangular waveguide step, even though the one considered would be only stepped in one of the axis, creating something similar to a stair shape.
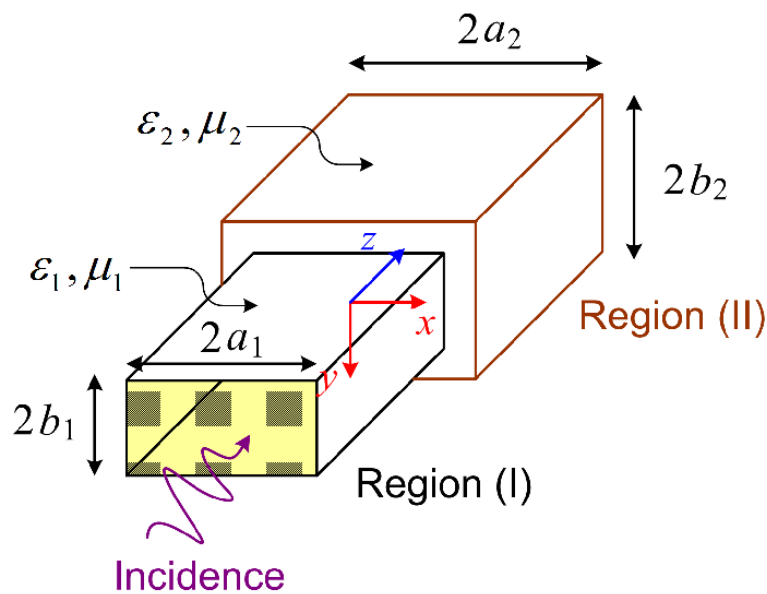
Figure 21: Geometry of a rectangular waveguide step.

[13]

This approach was seriously considered and even some articles like [13] showed how the transitions could be based on Chebyshev matching transformer. This looked really promis-

ing since we could parameterize the transition and find the best matching for our antenna.

Just when the simulations using this technique were about to start another idea came up. Since this new technique was much easier to explore, it was decided to give it a priority above the other two. This technique consists of one or more cylindrical screws which can be mechanically inserted into the center of the broad wall of a rectangular waveguide. For the dominant TE_{10} mode of propagation, the stub is then parallel to the electric field and appears as a shunting capacitive susceptance for stubs with diameters an order of magnitude smaller than the wide waveguide size.

Capacitive screw tuners can be broadly classified into two types. One design is the slide screw tuner, which has a single screw that can be moved both within and outside the waveguide as well as along its length. Over the entire waveguide bandwidth, the slide screw tuner is useful, but it has too much RF leakage for precise measurements. The multiscrew type with fixed position screws is the other variety of capacitive screw tuners. The construction of a screw spacing that makes the multi-screw tuner functional throughout a wide frequency range is the design challenge.

As it is explained in [15], depending on the waveguide that you are using, related to a certain range of frequencies, the location of the screws and the spacing between them varies. The waveguides and bands discussed in the book are up to 40 GHz, far from the band we are interested in. It is challenging to do a thorough mathematical analysis of a single or multiple variable-length cylindrical screws that extends from a rectangular waveguide's broad diameter. The literature [17] and [16] contains mathematical and experimental assessments of this issue, which are outside the scope of this project and will not be covered in this paper.

However, in the technique suggested in this book the highest frequency of the design band is considered first, in our case 80 GHz. Four stubs are spaced at 120° intervals. Physically this means $\lambda_g/6 + n\lambda_g/2$ at the highest frequency. The n $\lambda_g/2$ or an integral number of half wavelengths more than $\lambda_g/6$ spacing depends on the physical characteristics of the tuner. In most applications above 4GHz $\lambda_g/2$ must be added to $\lambda_g/6$ for spacing since the drive mechanisms used on these stubs cannot physically be spaced any closer together. At even higher frequencies λ_g or more may be needed. An example of the design technique is done for waveguide WR90 (8.2 - 12.4 GHz), which gives an idea of how the implementation of the technique is done.

Having all that in mind, the first prototype was done with just one screw to find out if with the most simple version of it, we could achieve our objectives. After a few optimizations, it was clear that the objective was going to be achieved. Table 2 contains the parameters of Prototype 6a and 6b. Both prototypes have the same dimensions, the only thing different between them is the number of screws used and their position.

Parameter	Prototype 6a	Prototype 6b
Width of waveguide section (mm)	3.0988	3.0988
Height of waveguide section (mm)	1.5494	1.5494
Length of waveguide section (mm)	2.84624	2.84624
Aperture width (mm)	16.2	16.2
Aperture height (mm)	1.15279	1.15279
Aperture length (mm)	8.027	8.027
Screw 1 Z axis position (mm)	1.961	0.996
Screw 1 Length (mm)	0.5539	0.53863
Screw 1 Z Radius (mm)	0.1	0.1
Screw 2 Z axis position (mm)	-	1.97414
Screw 2 Length (mm)	-	0.6595
Screw 2 Z Radius (mm)	-	0.1084

Table 2: Prototypes 6a and 6b parameters

In the appendix, you will be able to find the complete captures and results for both the prototypes 6a and 6b. Nevertheless, in figure 23 we can see the screw used in prototype 6a and the S11 result in 22, which reaches a value of -59.3 dB at the central frequency.

Similarly, in figure 25 we can see the screws used in prototype 6b and the S11 result in 24, which reaches a value of -76.2 dB at the central frequency.
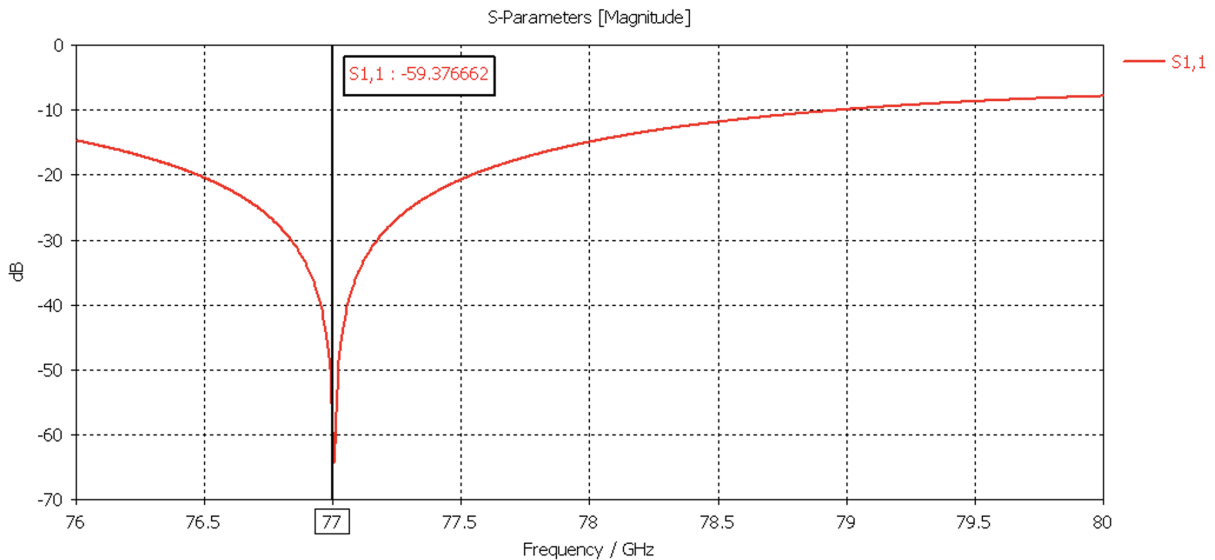
Figure 22: S11 graphic of Prototype 6a.

Obtaining these results was key to fulfilling the requirements of the antenna and moving the project forward. We had been stuck trying to reach an S11 value of -15 dB for weeks, and with the use of this technique in just a few days it was possible to achieve it. The screw technique proved to be a fast and simple way to adapt the antenna.
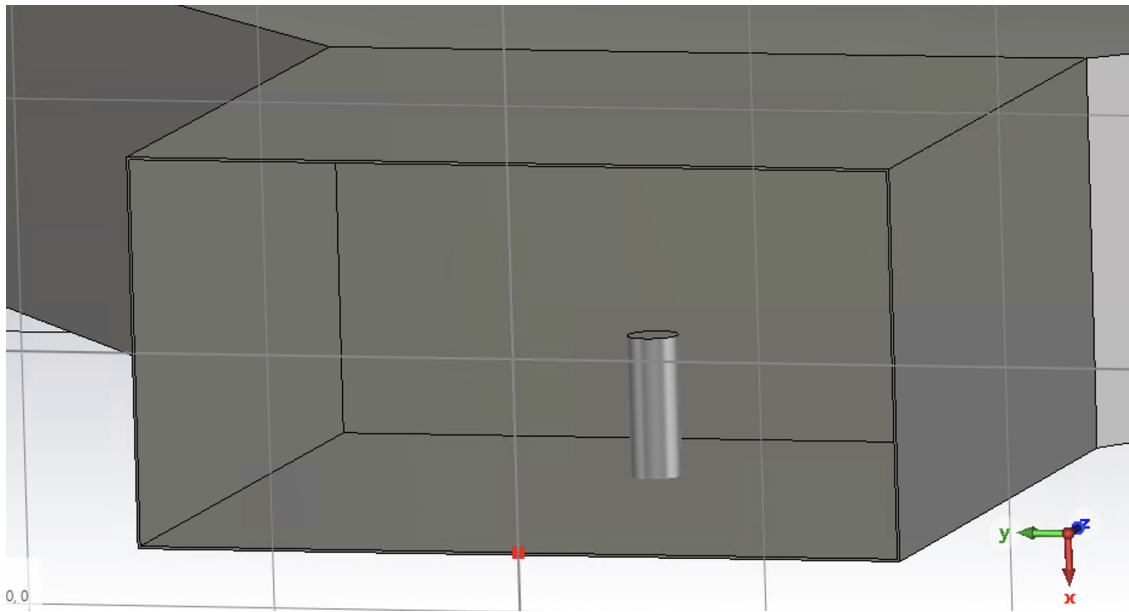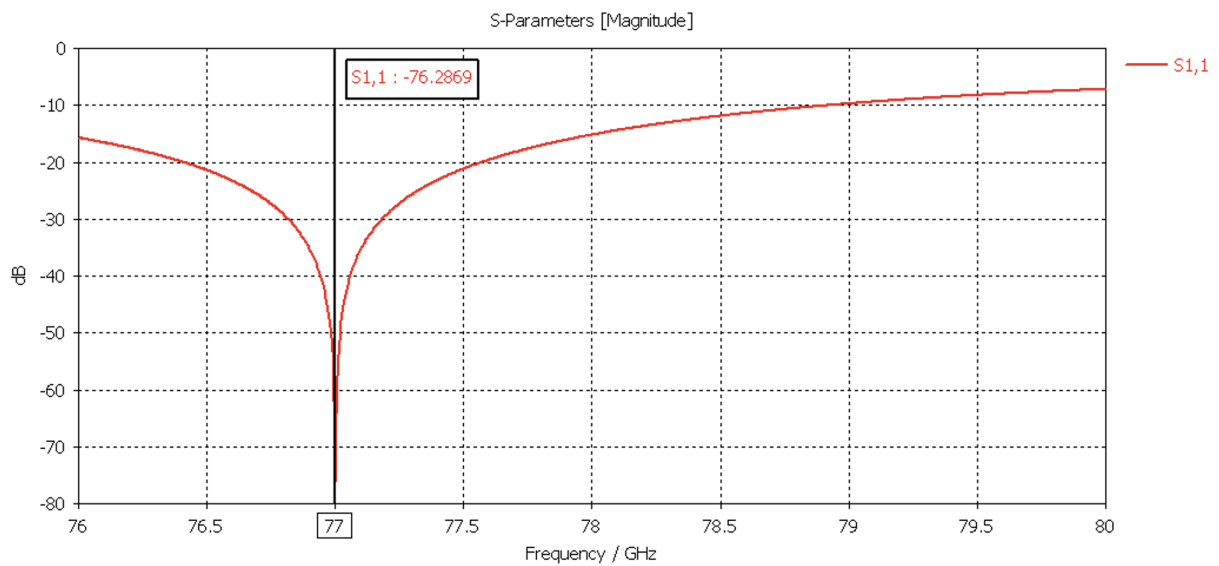
Figure 23: Screw used in Prototype 6a.

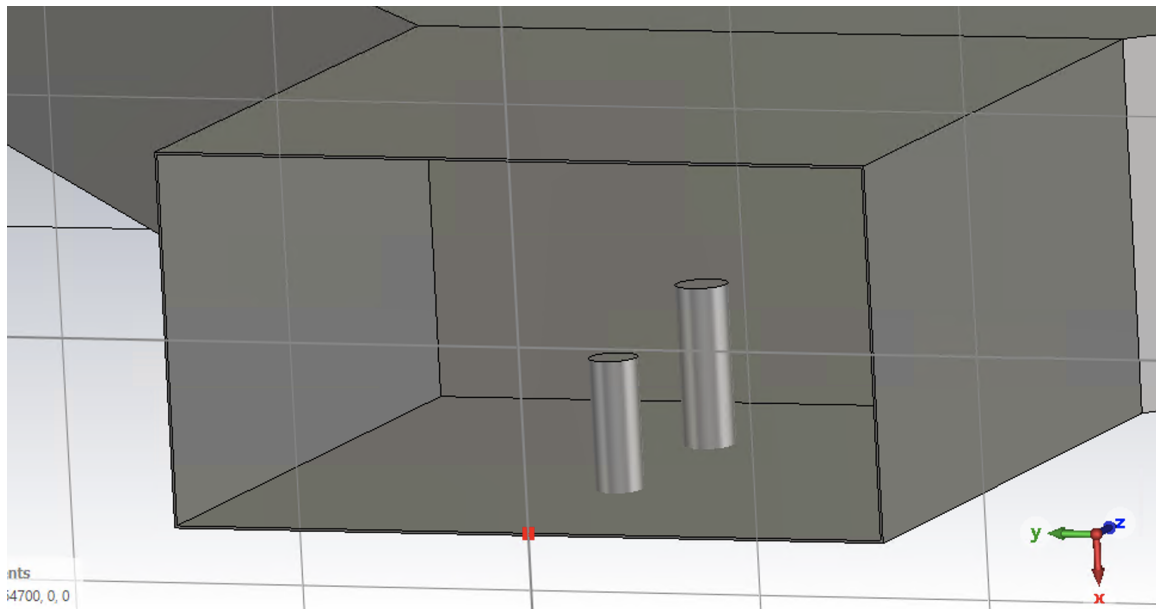Figure 24: S11 graphic of Prototype 6b.

Figure 25: Screws used in Prototype 6b.

4.3 Final phase

As we have stated in the design objectives, there is still the thickness issue that we hadn't addressed until this point, using until this point really thin walls of 0.1 mm. This is unrealistic from a mechanical point of view since the company's machinery could not fabricate it. After a meeting with the people in charge of manufacturing, a thickness of 0.5 mm was agreed upon. Knowing this, a new prototype was created with a waveguide, aperture, and screw of this thickness. The parameters of the final antenna can be seen in the table 3.

Parameter	Final antenna
Width of waveguide section (mm)	3.0988
Height of waveguide section (mm)	1.5494
Length of waveguide section (mm)	2.9385
Aperture width (mm)	16.95
Aperture height (mm)	0.49
Aperture length (mm)	8.027
Screw Z axis position (mm)	1.602
Screw Length (mm)	0.401
Screw Radius (mm)	0.5

Table 3: Final antenna parameters

In figure 26 and 27 we can observe the increment on the waveguide and the aperture walls, as well as in the screw radius. The increment in thickness affected the adaptation and the FOV in both the Elevation and Azimuth cuts, bringing it back below the objectives that were stated. For that reason, a new optimization of the parameters was made, modifying aperture values to reach the FOV objective first, and then the addition of a single screw to adapt the antenna again. In figure 26 and 27 we can observe the increment on the waveguide and the aperture walls, as well as in the screw radius. Even though two screws obtained a better S11 value, only one screw was used because there was not enough space to fit two. However, just one screw was enough to adapt the antenna to the central frequency, reaching -75 dB as is shown in figure 28.

The Elevation and Azimuth cuts have the FOV wanted as it can be seen in figures 29 and 30.

We can also observe the horizontal and vertical polarization in figures 31, 32 and overlapped in 33.
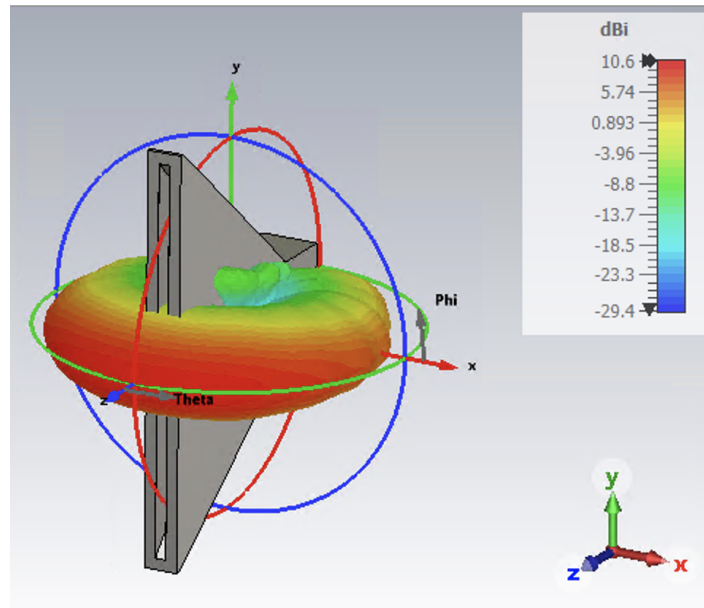
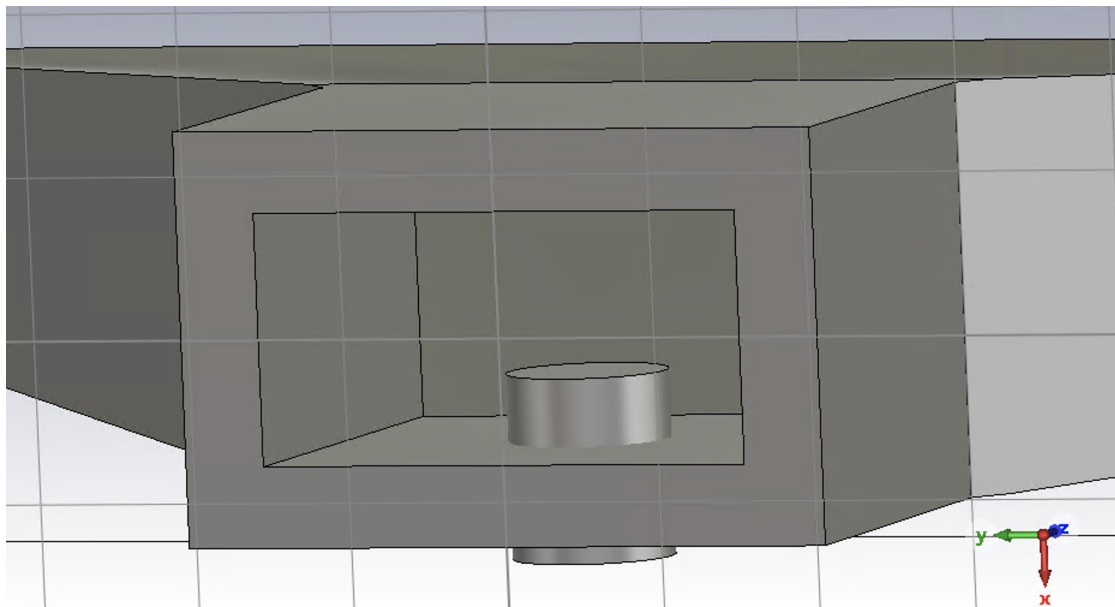Figure 26: Far-field of the final antenna design.

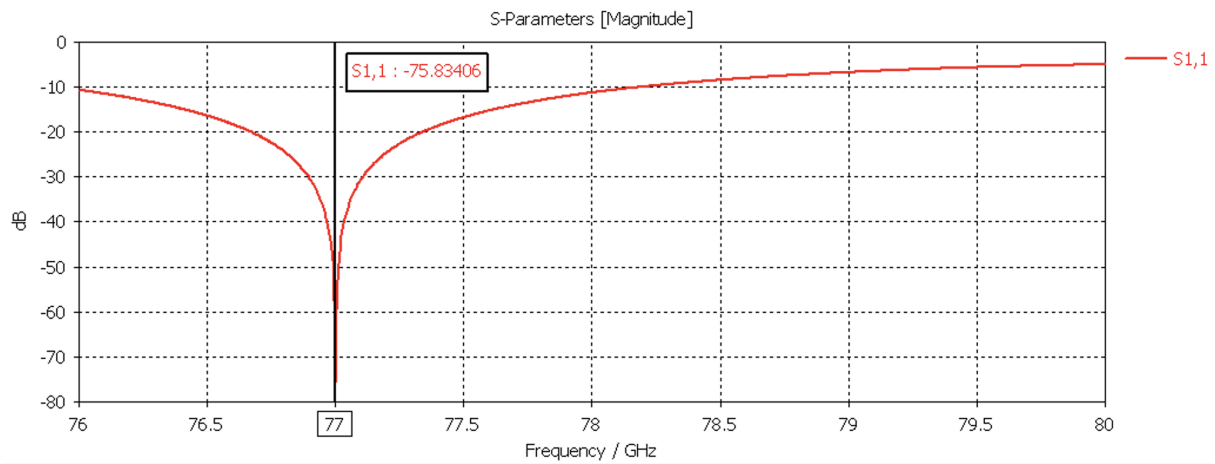Figure 27: Screw used in the final antenna design.

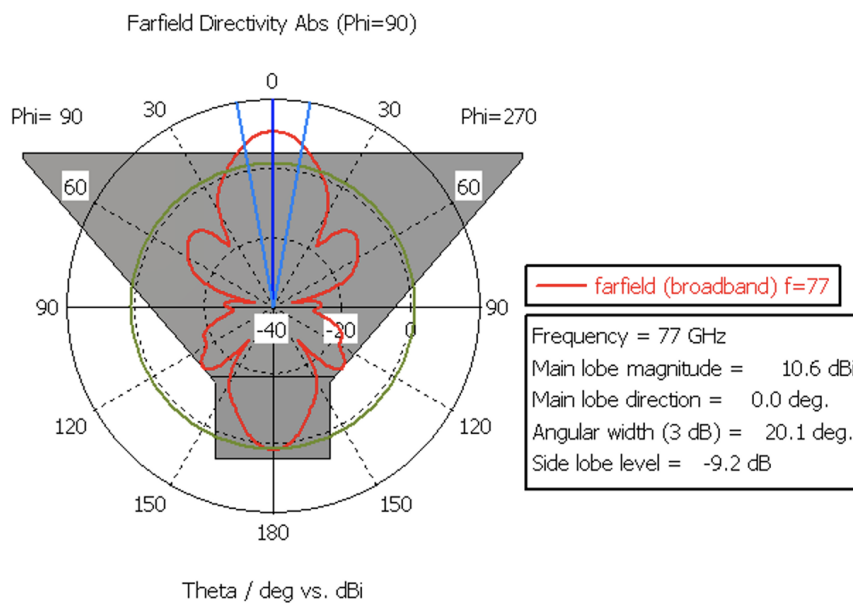Figure 28: S11 parameter of the final antenna design.

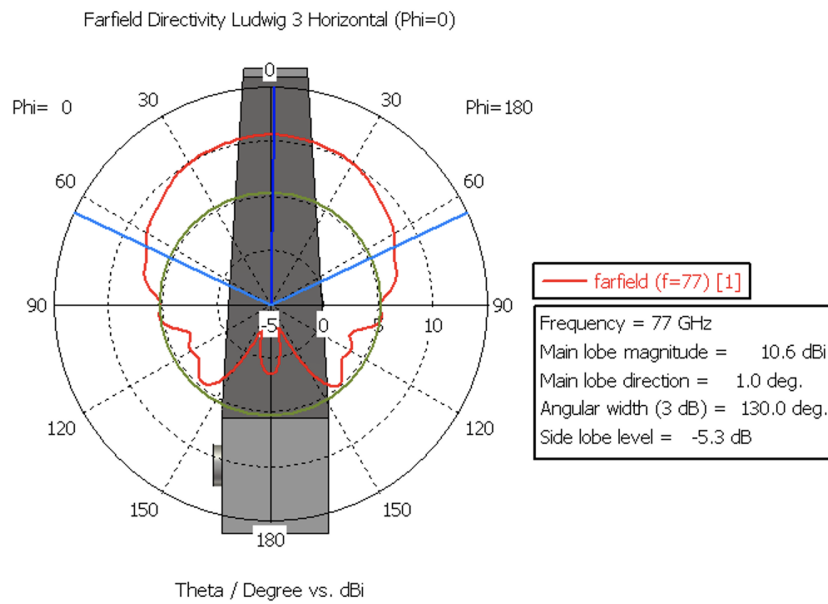Figure 29: Elevation cut of the final antenna design.

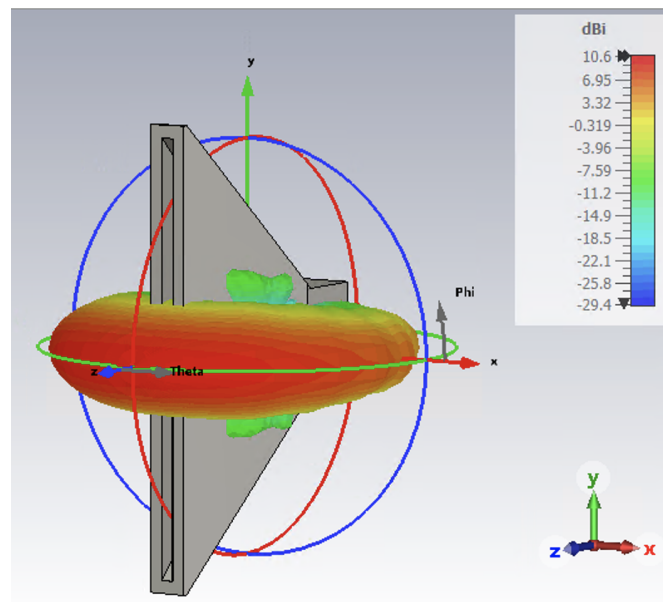Figure 30: Azimuth cut of the final antenna design.

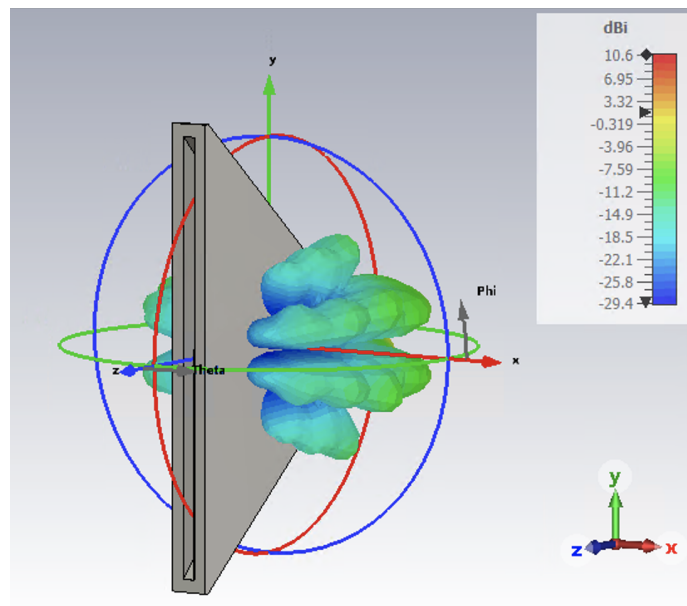Figure 31: Horizontal polarization (E_Theta) of the final antenna design.

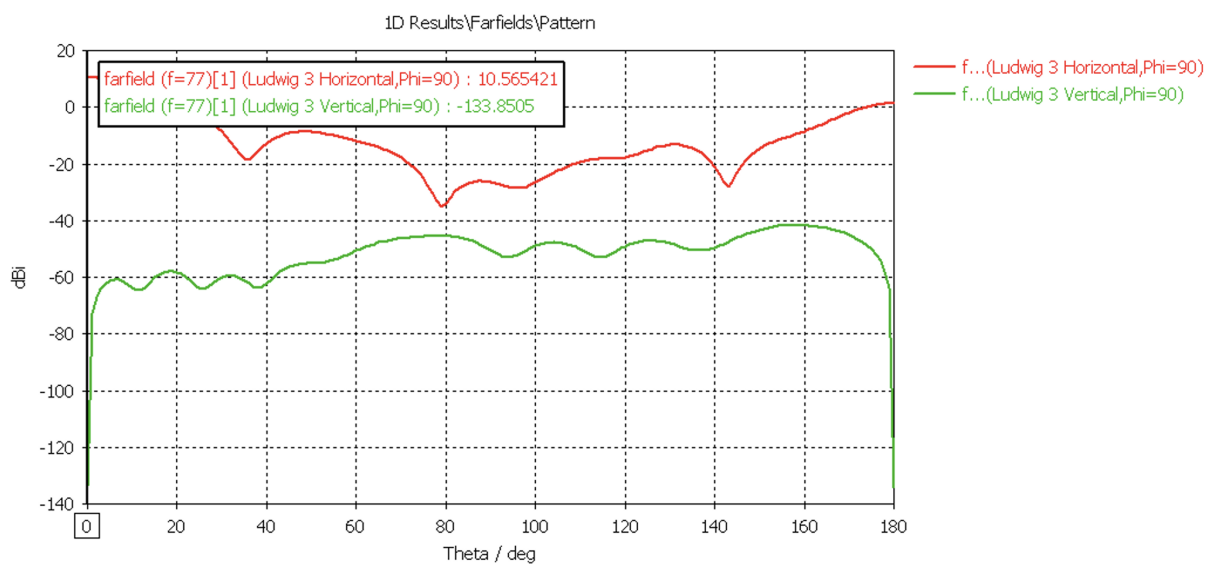Figure 32: Vertical polarization (E_Phi) of the final antenna design.

Figure 33: Horizontal and vertical polarization in boresight.

4.4 Antenna array review

The antenna array was not developed because the main requirements were accomplished with a single antenna and the company agreed. However, some simulations were done in order to observe its behavior of it and decide whether or not would be interesting to pursue this idea in future work.

In our case, an antenna array would have been used to accomplish the FOV on the elevation cut without having to increase that much the width since the use of an array is used for beam narrowing. Two different separations were used during the simulations, 1.5λ and 3λ, since they worked constructively in the main direction (more separations should be studied in the future). However, as can be seen in figure 37 and 39, increasing the distance creates new lobes in unwanted directions. Increasing the distance over 0.5λ leads to higher sidelobes. At the same time, you don't want to put the antennas too close to each other because that will restrain the aperture width that you can use in your antennas. For that reason, finding a good compromise between those two conditions would be key when optimizing the antenna. The elevation cut remains almost identical to the one obtained for the final antenna, which means that we wouldn't have to optimize the height of the antenna that much.
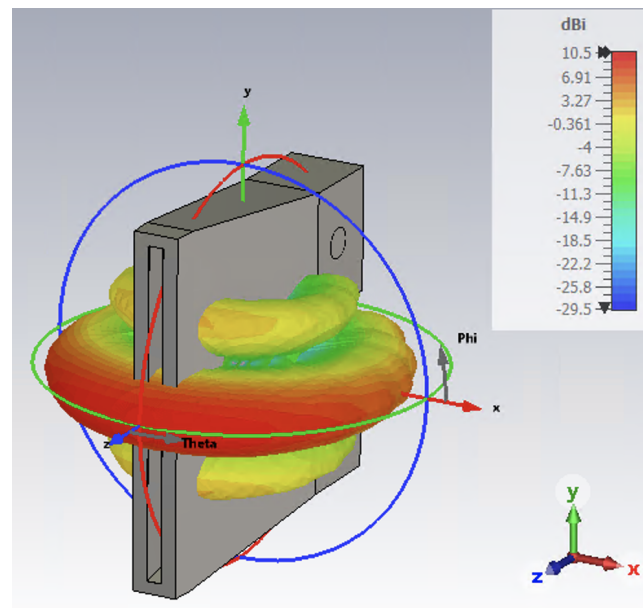

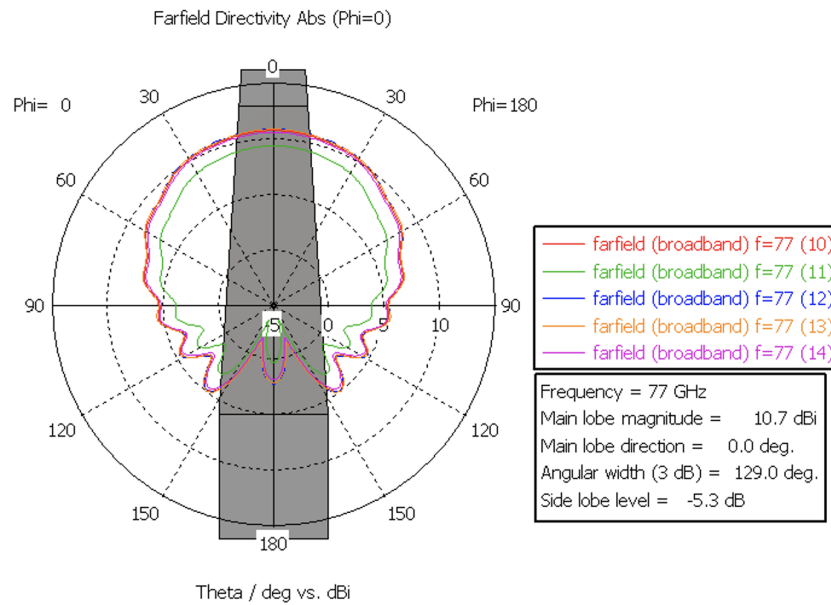Figure 34: Far-field of antenna array with separation of 1.5λ.

Farfield Directivity Abs (Phi=0)

Phi= 0

Phi=180

farfield (broadband) f=77 (10)
farfield (broadband) f=77 (11)
farfield (broadband) f=77 (12)
farfield (broadband) f=77 (13)
farfield (broadband) f=77 (14)

Frequency = 77 GHz
Main lobe magnitude = 10.7 dBi
Main lobe direction = 0.0 deg.
Angular width (3 dB) = 129.0 deg.
Side lobe level = -5.3 dB

Theta / deg vs. dBi

Figure 35: Azimuth cut of antenna array with separation of 1.5λ.

Farfield Directivity Abs (Phi=90)

Phi= 90

Phi=270

farfield (broadband) f=77 (10)
farfield (broadband) f=77 (11)
farfield (broadband) f=77 (12)
farfield (broadband) f=77 (13)
farfield (broadband) f=77 (14)

Frequency = 77 GHz
Main lobe magnitude = 10.7 dBi
Main lobe direction = 0.0 deg.
Angular width (3 dB) = 17.6 deg.
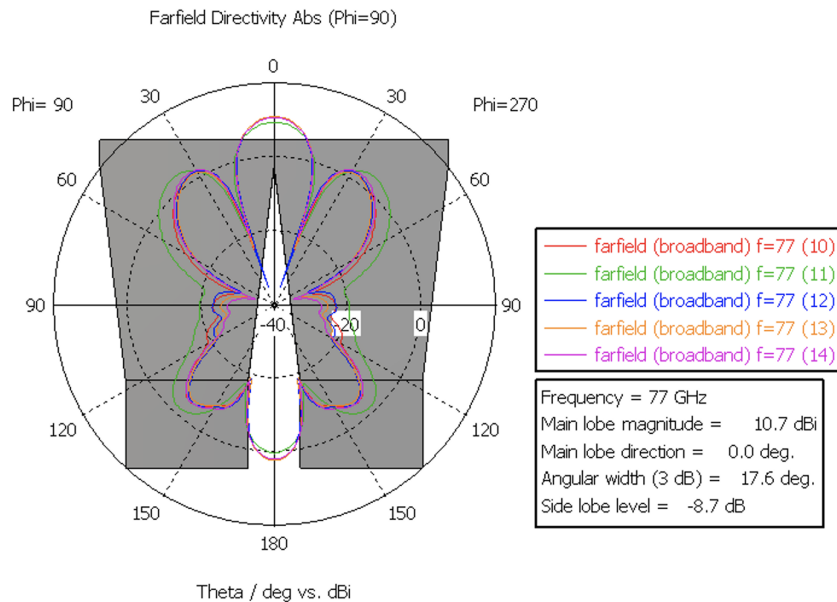Side lobe level = -8.7 dB

Theta / deg vs. dBi

Figure 36: Elevation cut of antenna array with separation of 1.5λ.

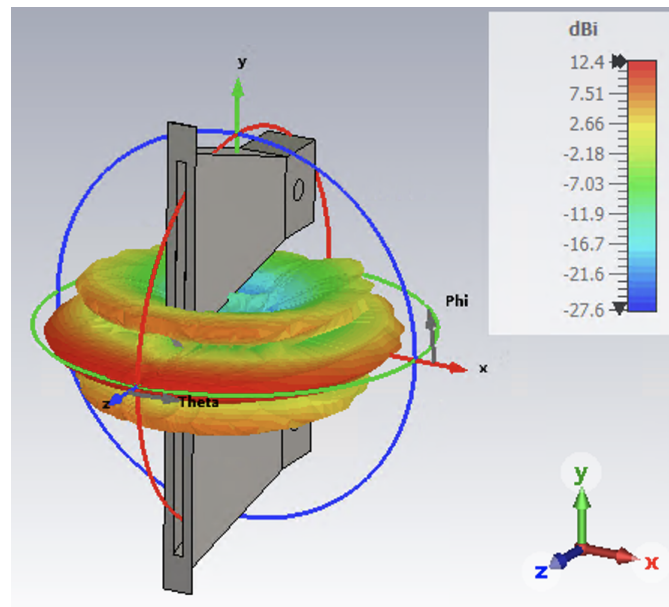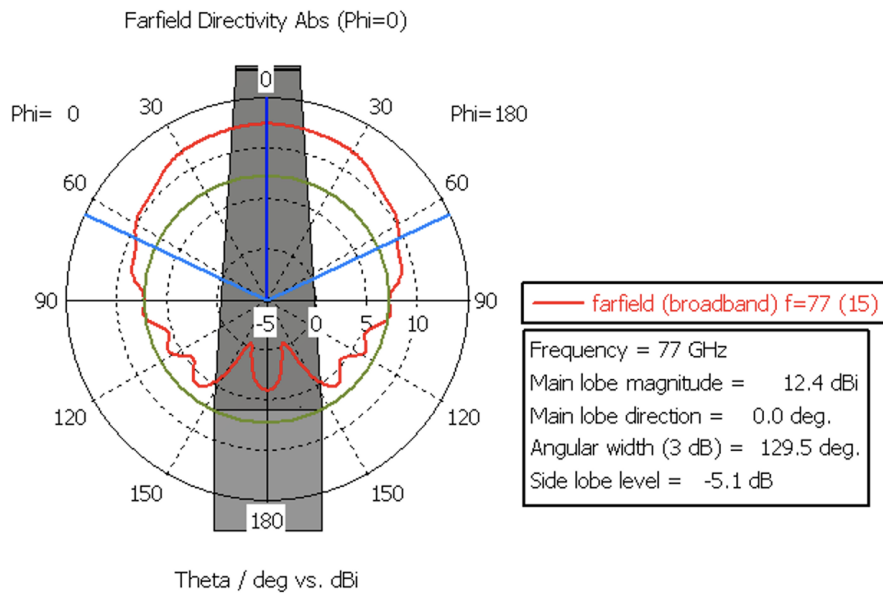Figure 37: Far-field of antenna array with separation of 3λ.

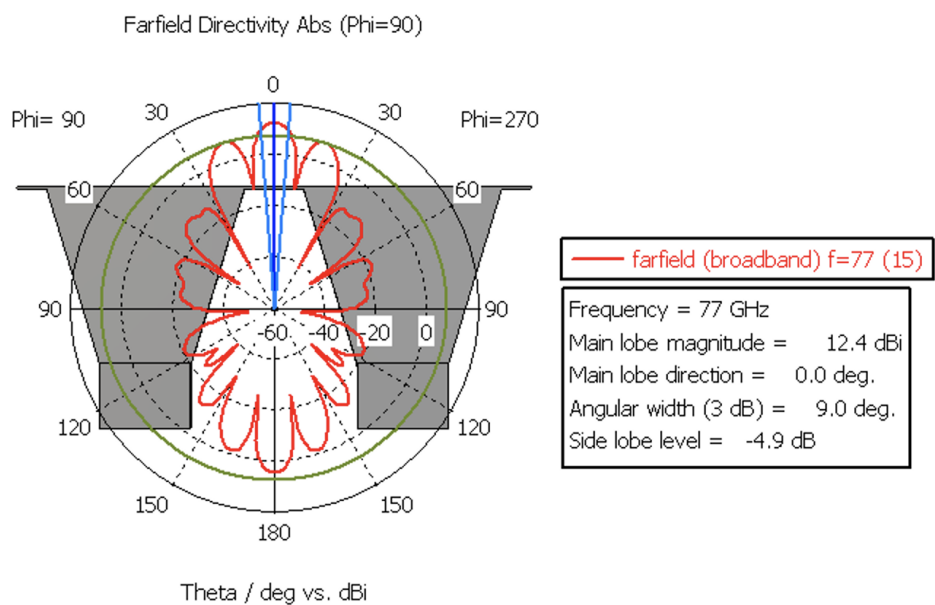Figure 38: Azimuth cut of antenna array with separation of 3λ.

Figure 39: Elevation cut of antenna array with separation of 3λ.

The results obtained looked promising and seemed like a feasible alternative to our design. However, no further optimizations were done since we had already achieved the objectives with a single horn antenna. Nevertheless, some advantages and drawbacks can be extracted from the observed behavior of the array:

- ADVANTAGES
  - Can potentially offer higher gain and directivity.
  - It offers beam steering electronically.
  - With the application of non-uniform input to each element, the radiation pattern can be shaped according to the requirement.

- DRAWBACKS
  - Increased feeding complexity.
  - Bulkier system
  - Larger separations could result in higher grating lobes (unwanted beams).
  - Increased resistive losses in the array.

5 Budget

The overall project development cost will be covered in this section. The student who created it and the professors/supervisors from both universities will incur the majority of the costs for carrying it out.

One CTU supervisor and one UPC tutor were involved in our case. The student must spend roughly 25 hours per credit, or roughly 750 hours total, to complete the 30 credits of the thesis. The CTU supervisor went for about an hour each week for a total of 12 weeks. About 14 hours of effort are thought to have been directly spent on this project, without including additional work for the evaluation. The projected amount of work for the UPC tutor, accounting for coordination and evaluation, is 8 hours per week because there is no ongoing weekly evaluation. The following table reveals the total budget, which is 10007 euros.

	Number	Salary (€/hour)	Hours	Salary (€)	Taxes (21%)	Total (€)
Student	1	10	750	7500	1575	9075
CTU Supervisor	1	35	14	490	103	593
UPC Supervisor	1	35	8	280	339	339
BUDGET						10007

Table 4: Table showing the budget considered during the development of the Thesis.

Since the student was given the option of working entirely remotely, there is no need to include an office space when calculating the materials portion of the budget. Instead, we must pay for the computer used. Taking into account that the student's computer costs 1.300€, has a 7-year (84-month) life expectancy, and a 25% residual value The amortizations can be determined as follows:

$$f = \frac{initialTotal - residualValue}{lifeExpectancy}$$

For the software used, we can't approximate the cost because it was not possible to obtain information regarding the price of the academic license. The cost of the material is as shown in the next table, where the use of them is of 5 months.

	Amount	Cost (€)	Initial total (€)	Residual value (€)	Amortization (€)	Total (€)
Computer	1	1500	1500	375	14	70

Table 5: Total amortization related to materials.

6 Conclusions and future development

This research is a comprehensive study of horn antennas working at EHF including a literature review, design, and simulation. Some general considerations were presented, common to all horn antennas working in this band. In addition, the requirements defined by the company were presented.

Several prototypes were designed and simulated, obtaining from each of them results that took the study one step closer to the final design. The knowledge obtained from the main prototypes was highlighted to explain the designing process.

After several months of designing, simulating, and optimizing prototypes, we concluded that a single antenna would be capable to achieve the requirements established by the company. For that reason, it was agreed to focus on the design of a single horn antenna, evaluating the possibility of designing an antenna array for future works.

Furthermore, the screw tuner technique used to adapt the antenna was key to achieving the objectives of the project. Before using it, we were stuck trying to achieve a reflection coefficient below -15 dB, and with the optimization of one or two screws, it was possible to achieve values of -75 dB at the central frequency.

In addition, after some simulations were completed, the antenna array showed great potential to be a viable alternative to also accomplish the demands. Due to focusing on the single antenna solution a final design was not developed. However, it would be interesting in possible future works to pursue this alternative and observe its boundaries and limitations.

In summary, this project should provide a clear view of how the design of the antenna was made and the design decisions that were taken to fulfill all the requirements agreed upon.

References

[1] Zbyněk Raida, Dušan Černohorský, Dalimil Gala, Stanislav Goňa, Zdeněk Nováček, Viktor Otevřel, Václav Michálek, Vlastimil Navrátil, Tomáš Urbanec, Zbyněk Škvor, Petr Poměnka, Jiří Šebesta, Geert Vanderstegen, Bart Vandijck, Bert Soors, Jeroen Schevernels, Javier Martín Del Valle, Martin Štumpf, Vladimír Seděnka, Peter Kovács, Jaroslav Láčík, Jana Jilková, Zbyněk Lukeš, and Michal Pokorný. 'Electromagnetic Waves Microwave Technique'. 2010.

[2] Akram Al-Hourani, Robin J. Evans, Peter M. Farrell, Bill Moran, Marco Martorella, Sithamparanathan Kandeepan, Stan Skafidas, and Udaya Parampalli. Chapter 7 - millimeter-wave integrated radar systems and techniques. In Rama Chellappa and Sergios Theodoridis, editors, *Academic Press Library in Signal Processing, Volume 7*, pages 317–363. Academic Press, 2018.

[3] Unknown. Kite aerial, signal hill, 1896.

[4] Unknown. Marconi's antenna system at poldhu, cornwall, 1901.

[5] John Belrose. 'fessenden and marconi: Their differing technologies and transatlantic experiments during the first decade of this century'. 9 1995.

[6] Peter Joseph Bevelacqua. 'antenna arrays: Performance limits and geometry optimization'. 5 2008.

[7] Vince Rodriguez. A brief history of horns. *In Compliance Magazine ISSN 1948-8254*, pages 26–29, 11 2010.

[8] Wikipedia contributors. Horn antenna — Wikipedia, the free encyclopedia. `https://en.wikipedia.org/w/index.php?title=Horn_antenna&oldid=1082054543`, 2022.

[9] Sophocles Orfanidis. 'Electromagnetic Waves Microwave Technique'. 2016.

[10] Wikipedia contributors. Extremely high frequency — Wikipedia, the free encyclopedia, 2022. [Online; accessed 7-December-2022].

[11] Ernestina Cianca, Marco Lucente, Tommaso Rossi, Cosimo Stallo, M. Ruggieri, and E Morelli. Ehf channel sounding for telecommunications applications via haps and balloons. 12 2022.

[12] CST Particle Studio. Waveguide port overview, 2013.

[13] Yong Heui Cho. Efficient electromagnetic boundary conditions to accelerate optimization of rf devices. *International Journal of Contents*, 7, 12 2011.

[14] Mohamed Mamdouh M. Ali, Shoukry I. Shams, and Abdel-Razik Sebak. Low loss and ultra flat rectangular waveguide harmonic coupler. *IEEE Access*, 6:38736–38744, 2018.

[15] Manly P Weidman and E. Campbell. 'A Method for Designing Multi-screw Waveguide Tuners'. 1970.

[16] Leon Lewin. 'Advanced Theory of Waveguides'. Iliffe and Sons, 1951.

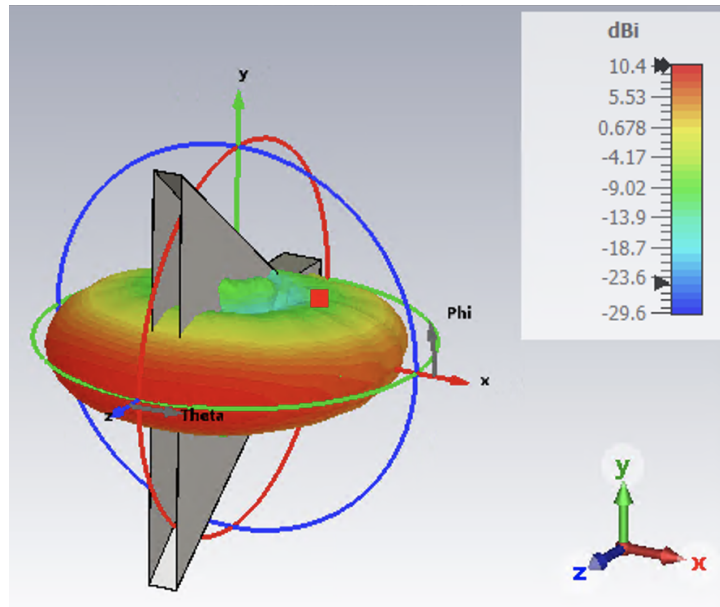[17] Nathan Marcuvitz. *Waveguide handbook*. Number 21. Iet, 1951.

Appendices

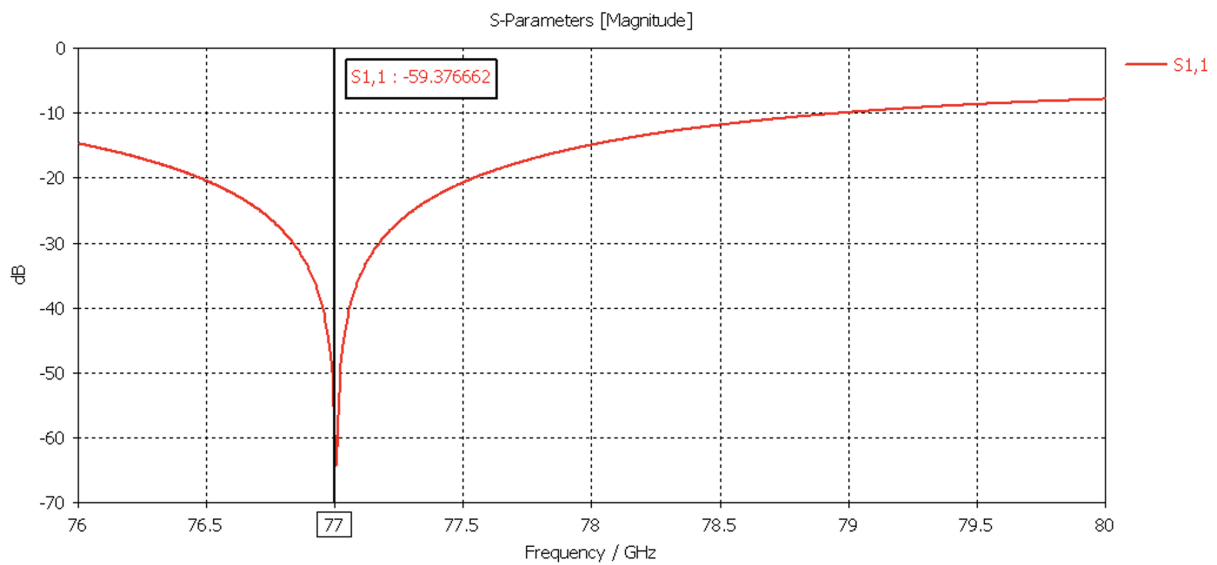Figure 40: Far-field of Prototype 6a.
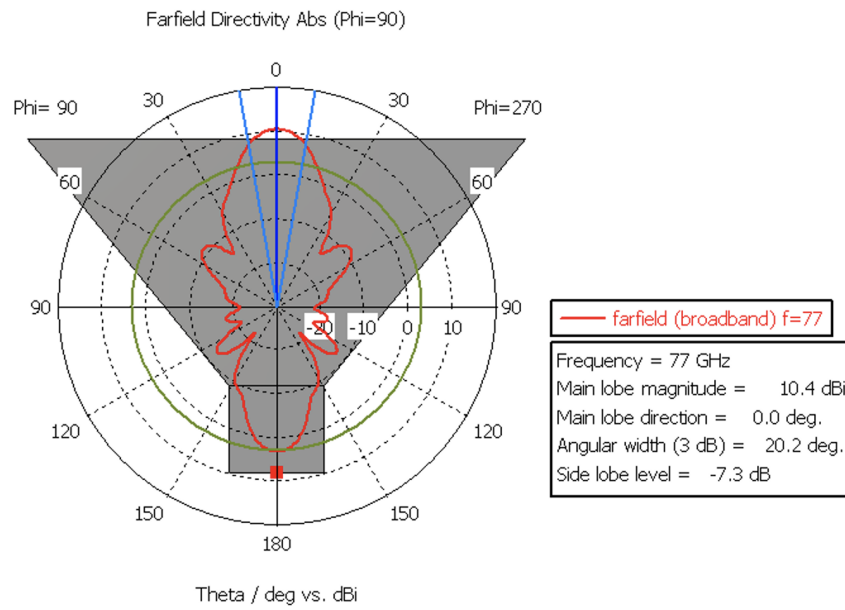

Figure 41: S11 graphic of Prototype 6a.

Farfield Directivity Abs (Phi=90)

Figure 42: Elevation cut of Prototype 6a.
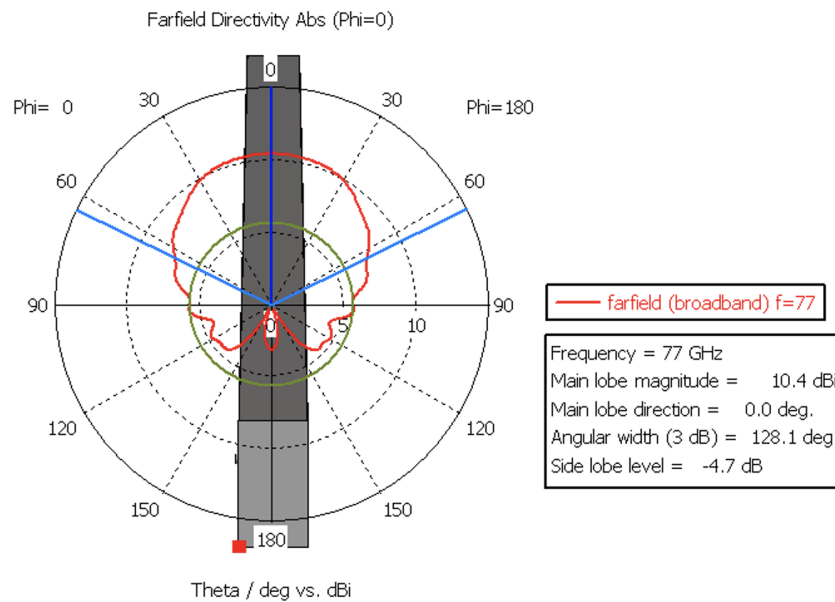
Farfield Directivity Abs (Phi=0)
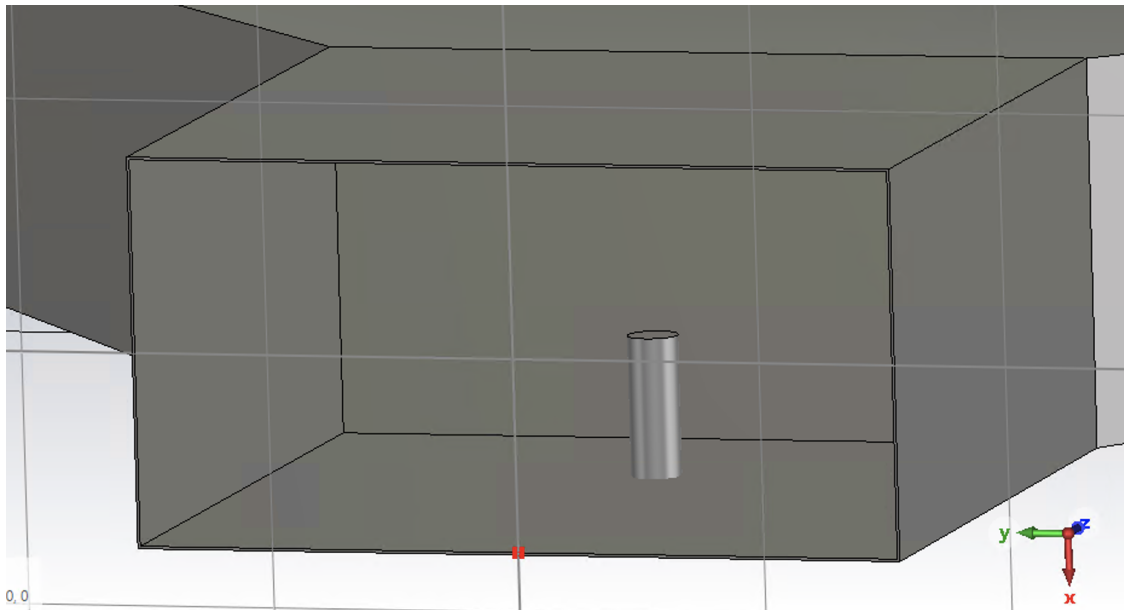

Figure 43: Azimuth cut of Prototype 6a.

Figure 44: Screw position in Prototype 6a.
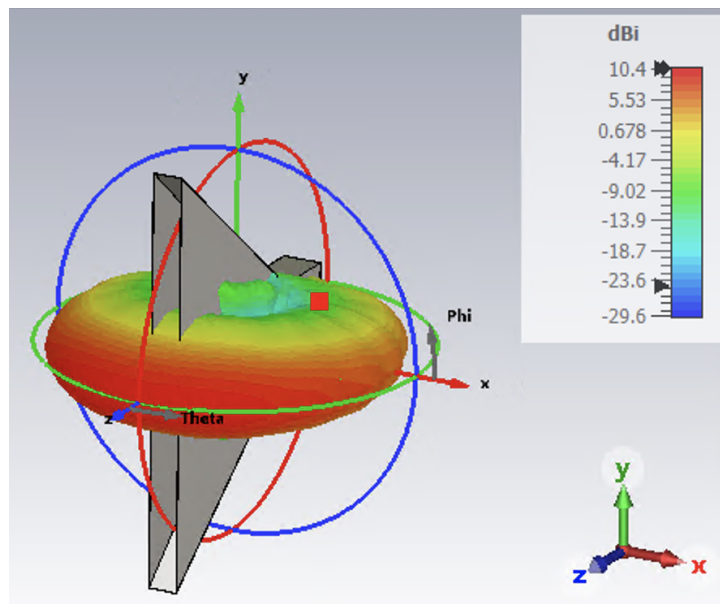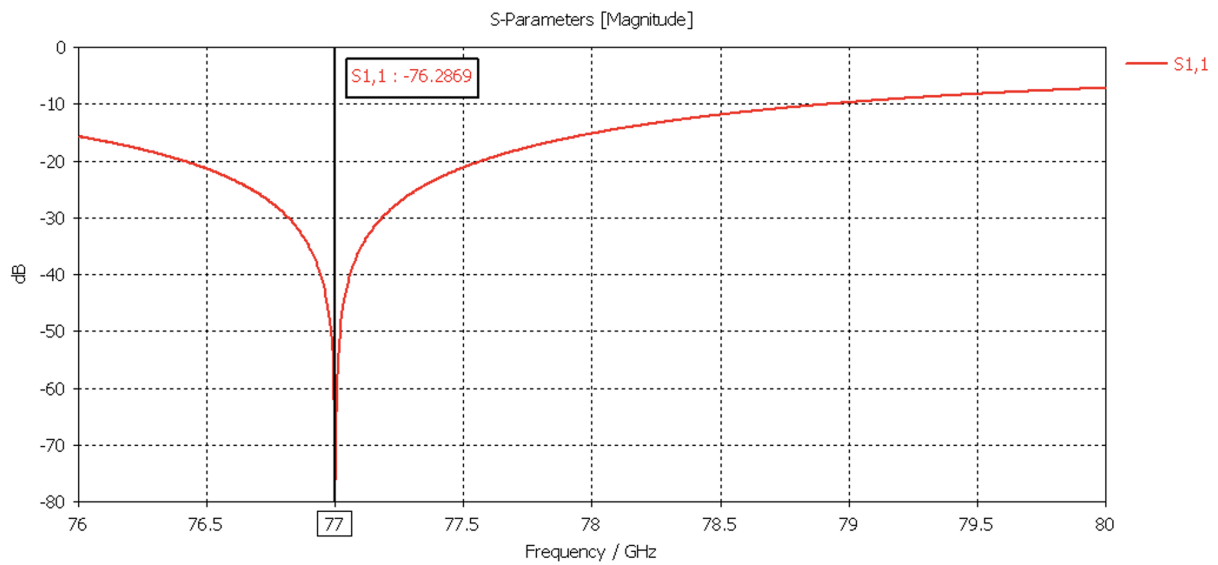

Figure 45: Far-field of Prototype 6b.
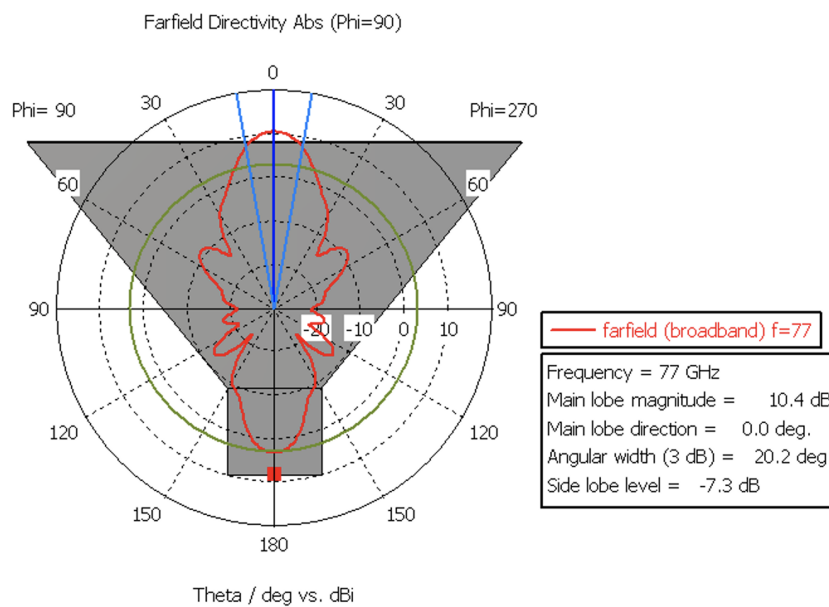
Figure 46: S11 graphic of Prototype 6b.

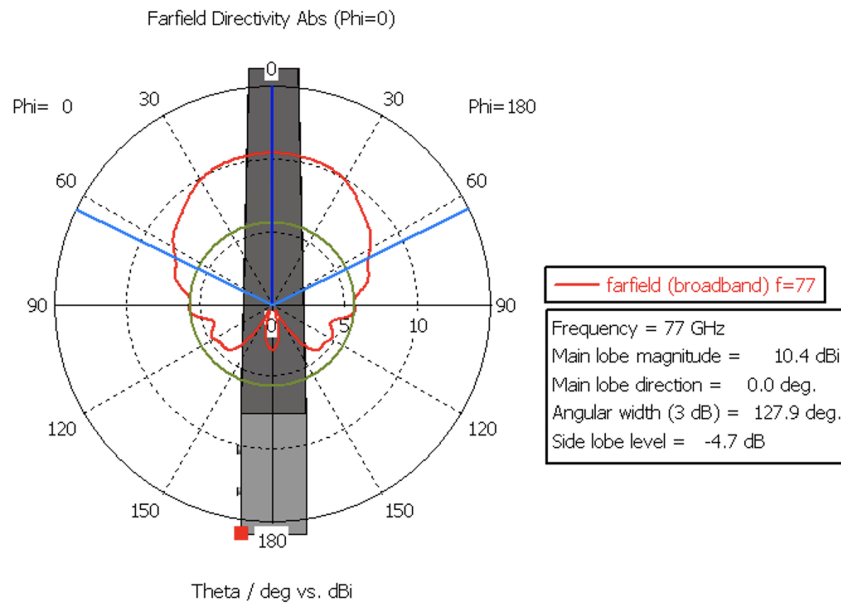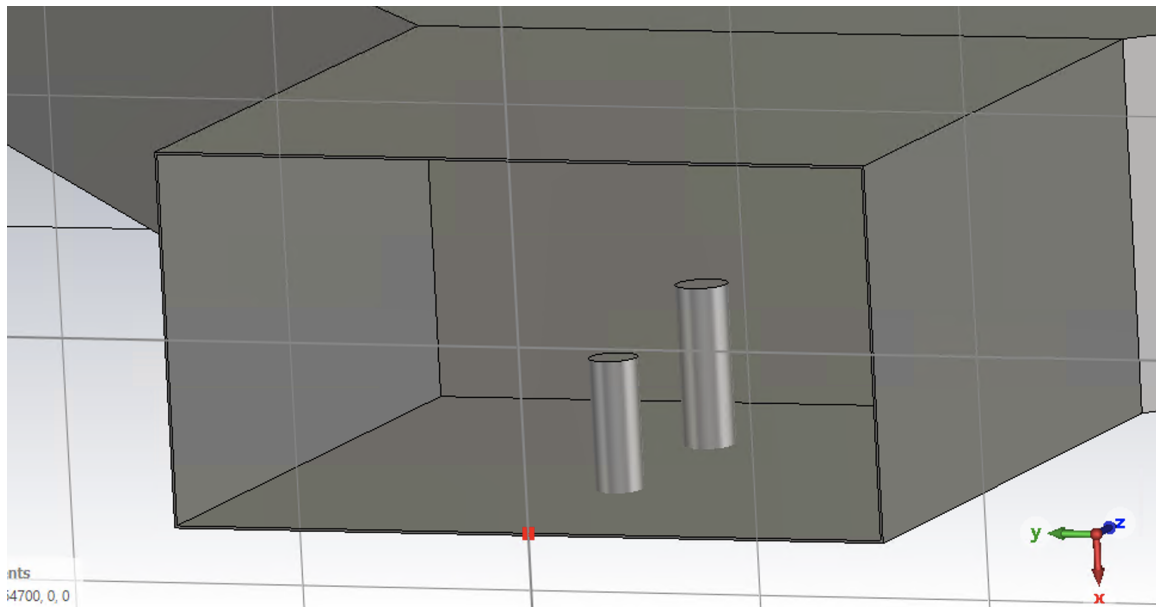Figure 47: Elevation cut of Prototype 6b.

Figure 48: Azimuth cut of Prototype 6b.

Figure 49: Screw position in Prototype 6b.